UNIVERSITÀ
DI PAVIA

Dipartimento di Biologia e Biotecnologie "L. Spallanzani"

Laurea Magistralis in Neurobiology

Exploring the relationship between microtubule instability and mitochondrial dysfunction in primary tauopathies

Analisi della relazione tra l'instabilità dei microtubuli e la disfunzione mitocondriale nelle tauopatie primarie

Supervisor:
Prof. Ilaria Maria Morella

Co-supervisor (s), if any:
Dr. Kathryn Bowles

Experimental thesis by
Anse Coekaerts

Academic Year 2025/2026

Abstract

Frontotemporal dementia is a heterogenous group of neurocognitive disorders. Increasing numbers of patients has been a concern over the past few years. Despite the increasing need, the exact pathological mechanisms leading to the development of frontotemporal dementia are still largely unknown, due to its heterogeneity and the complexity of neurodegenerative disorders in general. Understanding these key mechanisms is of crucial importance in treating and preventing frontotemporal dementia.

The heterogeneity of frontotemporal dementia indicates heterogeneity in the mechanisms involved in its development. In this thesis, we focused on frontotemporal dementia with tau-positive inclusion bodies, specifically those caused by a missense or synonymous mutation in the *MAPT* gene. These mutations result in mutant or wild-type 4R tau proteins, potentially affecting microtubule stability and mitochondrial function in different ways. The overall aim of this thesis is to better understand genotype-specific mechanisms and temporal changes caused by missense and synonymous mutations, using iPSC organoid lines.

Firstly, the impact on tau and its phosphorylation is determined by staining with PHF1 and DA9 in organoid lysates. Secondly, the relationship between mitochondria, microtubules and tau has been explored in this thesis. Impact of both mutations on the dynamics of microtubules, more specifically the ratio between stable and unstable tubulin, has been compared by imaging. The impact on mitochondria has been studied by looking at mitochondrial mass with PCR and quantification, flow cytometry (MitoTracker) and western blot (OXPHOS) and at mitochondrial functionality with flow cytometry (MitoSOX and TMRM) and western blot (OXPHOS). It has been hypothesized that mitochondria and tau impact each other in a two-way street: hyperphosphorylation could impact functionality of mitochondria and oxidative stress could impact hyperphosphorylation. This potential interaction is tested by western blots in mitochondria isolates (OXPHOS, PHF1, DA9) combined with results of the flow cytometry (MitoSOX and TMRM).

Missense mutation could mainly impact microtubule stability. Results showed imbalance in microtubule dynamics, with a phase of hyperstabilization, indicated by acetylation, potentially resulting in slower or halted mitochondrial transport. This early phase, characterized by hyperstabilization of tubulin, has been seen in previous studies as well and is possibly due to a compensatory mechanism in early stages, which is overcome by the rapid accumulation of tau into tangles in later stages. This early phase of hyperstable microtubules and potential switch to a later phase, characterized by unstable tubulin, could explain the early onset of symptoms and faster progression of the disease in patients with a missense mutation.

Even though mitochondrial mass was not impacted in either mutation over time compared to their wild-type control line, mitochondrial functionality was. Previous studies showed a relation between oxidative stress (MitoSOX) and phosphorylation of tau, indicated by significant changes in phosphorylation of tau protein (PHF1/DA9) in mitochondria isolates, mainly in synonymous mutations. The increase in oxidative stress and hyperphosphorylation in tau could indicate a role of two-way interaction between tau and mitochondria in synonymous mutations. Hyperpolarization of mitochondrial membrane was found in missense mutations at six months and in synonymous mutations at four months, which might be induced by different mechanisms in different mutations, namely changes in complex II in missense mutations and hyperphosphorylated tau in synonymous mutations. Findings from quantification of oxidative stress and mitochondrial membrane potential over time indicate that hyperpolarization of the mitochondrial membrane drives the generation of oxidative stress.

These results indicate potential genotype-specific mechanisms for the development of frontotemporal dementia. Synonymous mutations might cause frontotemporal dementia by the interplay between oxidative stress and hyperphosphorylated tau. The combination of increased acetylation of microtubules in early phases and live imaging results, indicating slow or blocked transport, suggest the impact of missense *MAPT* mutation on mitochondrial transport. Comparisons over time showed a potential cascade of mechanisms eventually leading to the development of frontotemporal dementia. Understanding genotype-specific neuropathogenesis and temporal changes of missense and synonymous *MAPT* gene mutations could lead to personalized treatment and early detection of the disease.

Abstract (Italian version)

La demenza frontotemporale costituisce un gruppo eterogeneo di disturbi neurocognitivi. Negli ultimi anni, l'aumento del numero di pazienti affetti ha destato preoccupazione. Nonostante le crescenti esigenze, i meccanismi patologici esatti che portano allo sviluppo della demenza frontotemporale sono ancora in gran parte sconosciuti, a causa della sua eterogeneità e della complessità dei disturbi neurodegenerativi in generale. Comprendere questi meccanismi chiave è di fondamentale importanza per il trattamento e la prevenzione della demenza frontotemporale.

L'eterogeneità della demenza frontotemporale indica un'eterogeneità nei meccanismi coinvolti nel suo sviluppo. In questa tesi ci siamo concentrati sulla demenza frontotemporale con corpi di inclusione tau-positivi, in particolare quelli causati da una mutazione missenso o sinonima nel gene MAPT. Queste mutazioni danno origine a proteine tau 4R mutanti o di tipo selvatico, che possono influenzare in modi diversi la stabilità dei microtubuli e la funzione mitocondriale. L'obiettivo generale di questa tesi è comprendere meglio i meccanismi specifici per genotipo e i cambiamenti temporali causati dalle mutazioni missenso e sinonime, utilizzando linee di organoidi derivati da cellule iPSC.

In primo luogo, l'impatto sui tau e sulla sua fosforilazione è stato determinato mediante colorazione con PHF1 e DA9 nei lisati degli organoidi. In secondo luogo, in questa tesi è stata esplorata la relazione tra mitocondri, microtubuli e tau. L'impatto di entrambe le mutazioni sulle dinamiche dei microtubuli, più specificatamente sul rapporto tra tubulina stabile e instabile, è stato confrontato mediante imaging. L'impatto sui mitocondri è stato studiato analizzando la massa mitocondriale mediante PCR e quantificazione, citometria a flusso (MitoTracker) e western blot (OXPHOS), nonché la funzionalità mitocondriale mediante citometria a flusso (MitoSOX e TMRM) e western blot (OXPHOS). È stata avanzata l'ipotesi che i mitocondri e la proteina tau si influenzino a vicenda in modo bidirezionale: l'iperfosforilazione potrebbe influire sulla funzionalità dei mitocondri e lo stress ossidativo potrebbe influire sull'iperfosforilazione. Questa potenziale interazione è stata verificata mediante western blot su isolati mitocondriali (OXPHOS, PHF1, DA9) in combinazione con i risultati della citometria a flusso (MitoSOX e TMRM).

La mutazione missenso potrebbe influire principalmente sulla stabilità dei microtubuli. I risultati hanno evidenziato uno squilibrio nella dinamica dei microtubuli, con una fase di iperstabilizzazione, indicata dall'acetilazione, che potrebbe comportare un rallentamento o l'arresto del trasporto mitocondriale. Questa fase iniziale, caratterizzata dall'iperstabilizzazione della tubulina, è stata osservata anche in studi precedenti ed è probabilmente dovuta a un meccanismo compensatorio nelle fasi iniziali, che viene superato dal rapido accumulo di tau in grovigli nelle fasi successive. Questa fase iniziale di microtubuli iperstabili e il potenziale passaggio a una fase successiva, caratterizzata da tubulina instabile, potrebbero spiegare l'insorgenza precoce dei sintomi e la progressione più rapida della malattia nei pazienti con una mutazione missenso.

Sebbene nel corso del tempo la massa mitocondriale non abbia subito variazioni in nessuna delle due mutazioni rispetto alla linea di controllo wild-type, la funzionalità mitocondriale ne è stata invece influenzata. Studi precedenti hanno evidenziato una relazione tra lo stress ossidativo (MitoSOX) e la fosforilazione della proteina tau, indicata da variazioni significative nella fosforilazione della proteina tau (PHF1/DA9) negli isolati mitocondriali, soprattutto nelle mutazioni sinonime. L'aumento dello stress ossidativo e l'iperfosforilazione della proteina tau potrebbero indicare un ruolo dell'interazione bidirezionale tra la proteina tau e i mitocondri nelle mutazioni sinonime. L'iperpolarizzazione della membrana mitocondriale è stata riscontrata nelle mutazioni missenso a sei mesi e nelle mutazioni sinonime a quattro mesi, il che potrebbe essere indotto da meccanismi diversi a seconda del tipo di mutazione, ovvero alterazioni del complesso II nelle mutazioni missenso e iperfosforilazione della proteina tau nelle mutazioni sinonime. I risultati della quantificazione dello stress ossidativo e del potenziale di membrana mitocondriale nel corso del tempo indicano che l'iperpolarizzazione della membrana mitocondriale determina la generazione di stress ossidativo.

Questi risultati indicano potenziali meccanismi specifici per genotipo nello sviluppo della demenza frontotemporale. Le mutazioni sinonime potrebbero causare la demenza frontotemporale attraverso l'interazione tra stress ossidativo e tau iperfosforilata. La combinazione tra l'aumentata acetilazione dei microtubuli nelle fasi iniziali e i risultati dell'imaging in vivo, che indicano un trasporto lento o bloccato, suggerisce l'impatto delle mutazioni missenso del gene MAPT sul trasporto mitocondriale. I confronti nel tempo hanno evidenziato una potenziale cascata di meccanismi che alla fine portano allo sviluppo della demenza frontotemporale. La comprensione della neuropatogenesi specifica per genotipo e dei cambiamenti temporali delle mutazioni missenso e sinonime del gene MAPT potrebbe portare a trattamenti personalizzati e alla diagnosi precoce della malattia.

Table of contents

Abbreviations

ATP	Adenosine triphosphate
BCA	Bicinchoninic Acid Assay
BSA	Bovine serum albumin
CHIP	Carboxy-terminus of Hsc70-interacting protein
Drp1	Dynamin-1-like protein
ECL	Enhanced chemoluminescence
ETC	Electron transport chain
FAD	Flavin adenine dinucleotide
FTD	Frontotemporal dementia
FUS	Fused in sarcoma
GDP	Guanosine diphosphate
GTP	Guanosine triphosphate
Hsp	Heat shock protein
(h)IPSC	Human induced pluripotent stem cells
MAPK	Mitogen-activated protein kinase
NAD(H)	Nicotinamide adenine dinucleotide (hydrogen, reduced form)
NFT	Neurofibrillary tangles
OXPHOS	Oxidative phosphorylation
PBS(T)	Phosphate-buffered saline (with Tween-20)
PCR	Polymerase Chain Reaction
PHF	Paired helical filaments

ROS	Reactive oxygen species
SIM	Structured illumination microscopy
TDP-43	TAR DNA-binding protein 43
TOMM40	Translocase of outer mitochondrial membrane 40
GAPDH	Glyceraldehyde 3-phosphate dehydrogenase
SDS-PAGE	Sodium dodecyl sulfate – polyacrylamide Gel electrophoresis
HRP	Horseradish peroxidase
WT	Wild-type
DNA	Deoxyribonucleic acid
RNA	Ribonucleic acid
DAPI	4’,6-Diamidino-2-phenylindole
TMRM	Tetramethylrhodamine, methyl ester
EBSS	Earle’s balanced salt solution
DMSO	Dimethyl sulphoxide
PHF1	Paired helical filament 1 (antibody)
DA9	Anti-total tau monoclonal antibody (clone DA9)
SSC-A	Side scatter – area
FSC-A	Forward scatter – area
FSC-H	Forward scatter – height
VL1-A	Violet laser 1 – area
MAPT	Microtubule-associated protein tau
Miro	Mitochondrial Rho GTPase

MAP1A	Microtubule-associated protein 1A
PINK1	PTEN-induced kinase 1
TBS	Tris-buffered saline
CHAPS	3-[(3-cholamidopropyl)dimethylammonio]-1-propanesulfonate
RIPA	Radioimmunoprecipitation assay
GSK3β	Glycogen synthase kinase-3β

1. Introduction

Frontotemporal dementia (FTD) is the leading cause of early-onset dementia, in which symptoms are present before 65 years old (Hendriks et al., 2021). According to analysis by Urso et al. (2025), FTD has a prevalence of 9.17 per 100.000 people globally with an expected increase over the following years according to the World Health Organisation (Bang et al., 2015). So, it is of significant importance to gain a better understanding of the pathophysiology of the disease to be able to control and treat the disease in a better manner.

FTD is a heterogenous group of neurocognitive disorders affecting the frontal cortex and the temporal cortex (Bang et al., 2015). In approximately 35-50% of FTD patients, tau can be found in the abnormal inclusion bodies (Baborie et al., 2011; Bang et al., 2015; Boxer et al., 2013). Tau is a microtubule-associated protein (Goedert, 1993) and its hyperphosphorylation has been hypothesized to play an important role in the development of FTD. However, in this thesis, we would like to understand the exact mechanisms leading to FTD-tau in different FTD-related *microtubule-associated protein tau (MAPT)* gene mutations. The impact of an increase in mutated 4R tau proteins due to a missense *MAPT* mutation or an increase in wild-type 4R tau proteins at early stage of development due to a synonymous *MAPT* gene mutation was studied in this thesis. Firstly, the impact on tau, tubulin and their interaction was studied to understand how exactly mutations in tau could induce microtubule instability. Secondly, this thesis studied the potential impact of these mutations on mitochondria and the interaction between mitochondria and tau proteins. This could give us insights on how both mutations could lead to neurodegeneration in the frontal and temporal cortices causing FTD.

1.1 Frontotemporal dementia

FTD is a group of neurodegenerative diseases affecting the frontal and temporal cortex and is characterized by progressive deficits in executive function, language and/or behavior. It is a heterogenous group in scope of clinical presentation, genetic background and pathology (Bang et al., 2015). The frontal cortex has a role in higher-order cognitive abilities and in initiating and directing physical movements. Deficits in the frontal cortex have played a role in several psychiatric diseases and could alter personality. The frontal cortex can receive input from sensory and motor cortices, thalamus, and brainstem. It sends outputs to the hippocampus, basal ganglia, cerebellum, thalamus, and other associated cortices (Buchsbaum, 2004). The frontal cortex is also connected to the temporal cortex which involves the language areas (Faw, 2003).

The temporal cortex can be subdivided into different cortices with several distinct functions. First of all, the superior temporal gyrus is part of the temporal cortex (Kiernan, 2012). This region is important for auditory processing and language comprehension. It houses the primary auditory cortex, decoding pitch, volume and frequency, and Wernicke's area, decoding receptive language and semantic speech comprehension (Binder, 2015; Carl Wernicke, 1874; Kiernan, 2012). Secondly, the temporal cortex also includes the inferior temporal cortex, involved in the ventral visual pathway or the "what" pathway (Kravitz et al., 2013), and the fusiform gyrus, involved in face recognition (Kanwisher et al., 1997). Lastly, the temporal cortex contains the medial temporal cortex, consisting of the hippocampal region, perirhinal, entorhinal, and the parahippocampal cortices, essential for episodic memory (Kurz et al., 2014).

FTD has been subdivided into three variants based on symptoms, caused by specific patterns of atrophy: behavioural frontotemporal dementia, non-fluent primary progressive aphasia and semantic primary progressive aphasia (Gorno-Tempini et al., 2011). Behavioural FTD is characterized by a decline in interpersonal and executive skills. This is accompanied by a change in emotional responsivity and other abnormal behaviours (Warren et al., 2013). Magnetic resonance images have been variable in patients with behavioural FTD showing asymmetric atrophy between hemispheres in frontal cortex and anterior temporal cortex in the majority of patients, while the posterior cortical areas are often less affected. An early indicator of behavioural FTD could be the atrophy of the orbitofrontal cortex (Perry et al., 2006; Warren et al., 2013). Non-fluent primary progressive aphasia is characterized by a progressive decline in the ability of a person to express themselves through language, accompanied by non-fluent speech (Rohrer, Rossor, et al., 2010). In non-fluent primary progressive aphasia, mainly the perisylvian cortices in the dominant hemisphere are affected. This region is involved in speech production (Rohrer, Ridgway, et al., 2010). Also in this variant, the

degree of atrophy in the brain regions differ significantly among patients (Warren et al., 2013). Lastly, the semantic primary progressive aphasia impacts the semantic memory (Hodges & Patterson, 2007). In contrast to the other two variants, semantic primary progressive aphasia has a remarkably uniform neuroanatomic profile. Magnetic resonance imaging shows asymmetric atrophy of the anteroinferior temporal cortex. As the disease progresses, atrophy extends into the two hemispheres and into posterior temporal and inferior frontal cortices (Rohrer et al., 2009; Warren et al., 2013).

FTD can also be subdivided into variants according to the protein involved in neuropathogenesis, namely tau, fused in sarcoma (FUS) protein or transactive response deoxyribonucleic acid (DNA)-binding protein, 43kD (TDP-43). FTD-TDP43 is the most common variant, accounting for approximately 50% (Bang et al., 2015). TDP-43 is a DNA/RNA-binding protein, involved in many steps of ribonucleic acid (RNA) processing (Buratti & Baralle, 2010). However, the precise function in the brain is still unknown (Mackenzie & Neumann, 2016). Accumulation of TDP-43 has been seen in most FTD cases with inclusions that are tau-negative and ubiquitin-positive. TDP-43 proteins showed abnormal modifications, including hyperphosphorylation, which could explain their aggregation (Arai et al., 2006; Neumann et al., 2006). FTD-TDP43 can be further subdivided into four groups based on clinical and genetic correlation (Mackenzie & Neumann, 2016), reiterating the heterogeneity of FTD. Secondly, FTD-FUS, caused by a mutation in the *FUS* gene, accounts for approximately 10% of FTD cases (Mackenzie et al., 2011). FUS protein is also a DNA/RNA-binding protein involved in many RNA and DNA processes and is indicated to have a role in neuronal plasticity and maintenance of dendritic integrity within neurons (Neumann et al., 2009). FTD-FUS can be subdivided into three different rare diseases (Josephs et al., 2011). Lastly, there is FTD-tau which accounts for 35-50% of FTD patients (Baborie et al., 2011; Bang et al., 2015; Boxer et al., 2013). Also, this group of FTD variants can be further subdivided into different subtypes, of which corticobasal degeneration is the most common (Josephs et al., 2011). FTD-tau is the focus of this thesis, more specifically FTD caused by an increase in either mutated or wild-type 4R tau proteins.

1.2 Tau

Tau protein is a microtubule-associated protein, which is encoded by the *MAPT* gene. This gene is located on chromosome 17 in humans, more specifically on the long arm, and consists of 16 exons (Goedert, 1993). The gene results in many isoforms, produced by alternative splicing of its mRNA precursor. These different variants can influence the aggregation abilities of tau, which is associated with many neurodegenerative diseases (Himmler, 1989; Yang et al., 2024).

The sequence of the *MAPT* gene consists of an N-terminal region, a proline-rich domain, microtubule-binding repeats, and a C-terminal domain. In the human central nervous system, variations in the N-terminal region, containing two distinct alternatively spliced N-terminal inserts, and the repeats are responsible for six different isoforms, formed due to alternative splicing of exons 2, 3 and 10. These isoforms are 4R0N, 4R1N, 4R2N, 3R0N, 3R1N and 3R2N (figure 1) (Goedert et al., 1998; T. Guo et al., 2017). Depending on the developmental stage, different isoforms might be present in the brain. In foetal human brains, only the 3R0N isoform is expressed, while in adult human brains, all isoforms are present (Goedert et al., 1989; Trabzuni et al., 2012). The ratio between 3R and 4R tau proteins can differ between different cells but should be maintained within those cells for physiological functioning. An alteration in this ratio between 3R and 4R tau, due to an increase of 4R tau, has been linked to multiple primary tauopathies (Buchholz & Zempel, 2024; Trabzuni et al., 2012).

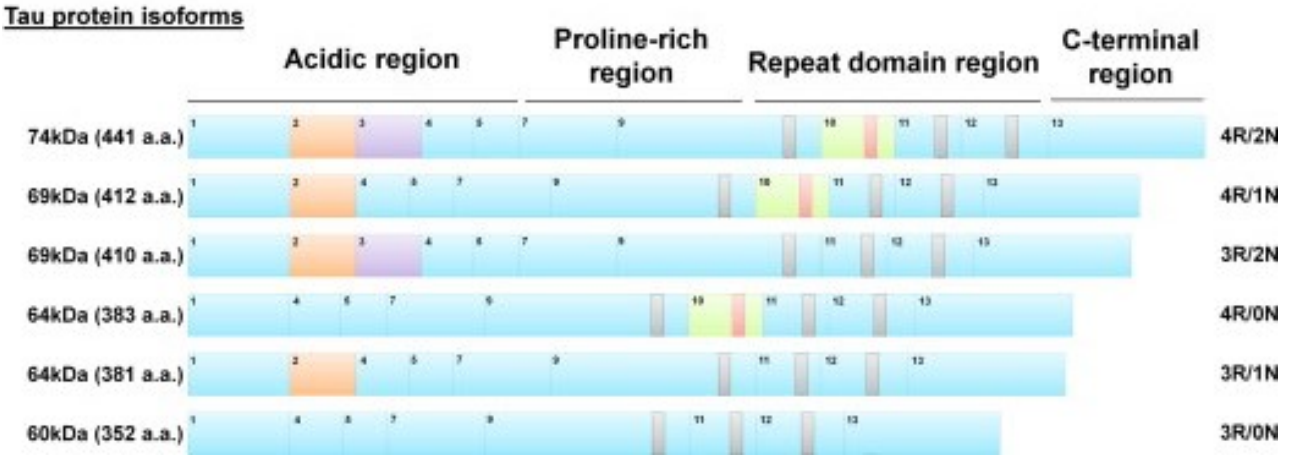

Figure 1: In adult human brains, tau is expressed as six distinct isoforms, due to alternative splicing of its mRNA precursor. The inclusion of exon 2 (orange) and/or exon 3 (purple) determines the number of N-terminal inserts while the alternative splicing of exon 10 (yellow) determines the number of C-terminal repeat domains. The repeat domain region, responsible for binding microtubules, consist of four repeat domains: R1, R3, R4 (grey) and R2 (red). This last repeat domain (R2) is only included in 4R tau proteins (Martin et al., 2011).

Tau is subjected to many different post-translational modifications like phosphorylation. Phosphorylation is one of the most studied post-translational modifications of tau, which contains 85 putative phosphorylation sites (T. Guo et al., 2017; Hanger et al., 2009). The overall consensus is that hyperphosphorylation of tau could be involved in pathogenesis of tauopathies. This hypothesis is based on the increased levels of tau phosphorylation observed in all tauopathies. Previous research has also shown that phosphorylation occurs prior to or at the same time as other post-translational modifications and prior to aggregation, suggesting that phosphorylation is an initiating event in tauopathies. Despite these results, it is still unclear if there is an actual causative relationship between phosphorylation, other post-translational modifications, and aggregation (Noble et al., 2013).

Hyperphosphorylation could limit the affinity to bind microtubules and allows them to form paired helical filaments (PHF), which can be formed by all six isoforms (Goedert et al., 1992; von Bergen et al., 2000). This soluble tau is sensitive to additional post-translational modifications, which can promote tau dimerization in an anti-parallel manner by altering its structure. When these tau structures are stable, they can form oligomers and further on protomers. Two protomers that are in proximity will form PHFs and eventually neurofibrillary tangles (NFT) (figure 2) (Martin et al., 2011; Meraz‐Ríos et al., 2010). The tau oligomers are hypothesized to have the ability to spread from cell to cell through prion-like aggregation. This could induce misfolding of healthy tau, which leads to the formation of new oligomers in neighbouring cells and consequently could result in the spread of misfolded tau throughout different brain areas (Jucker & Walker, 2013).

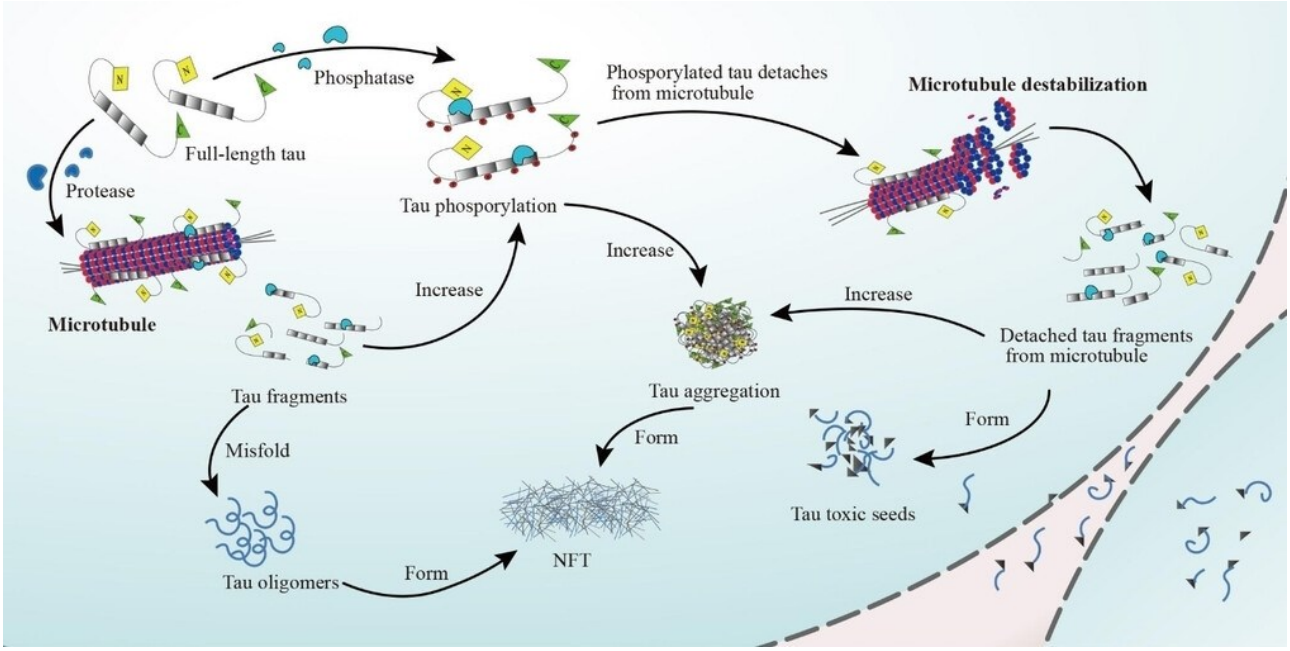

Figure 2: Tau hyperphosphorylation could potentially adjust the structure of tau, causing it to lose its ability to bind to microtubules. The microtubules become instable and tau becomes soluble. Soluble tau can undergo further post-translational modifications, which further adjusts the structure of tau. This could promote the dimerization of tau, leading to the formation of oligomers, protomers, paired helical filaments and eventually neurofibrillary filaments. Tau oligomers might have the ability to spread and impact tau in other cells via a prion-like aggregation mechanism (Di Lorenzo, 2024). Abbreviations: NFT: neurofibrillary filaments

Tau aggregation might have a role in neurodegeneration due to the instability of microtubules. However, tau phosphorylation might influence neurodegeneration in other ways as well. Phosphorylated tau might induce tau misplacement from axons to the somatodendritic compartment. This might compromise axonal microtubule integrity and can induce synaptic dysfunction (Hoover et al., 2010). Tau phosphorylation can also disrupt its own intracellular route of degradation by interrupting its recognition by CHIP-HSP90 complex, which protects the tau protein from degradation by the proteasome (Dickey et al., 2007). The microinjection of tau into the synaptic terminal has also been proven to cause increase of calcium which in its turn disrupts synaptic transmission (Moreno et al., 2016). Lastly, phosphorylation could alter the connection between tau and its interacting partners which disturbs the functioning of tau in signalling pathways (Hanger et al., 2009). Even though there may be multiple routes by which pathogenic tau impairs cellular health, evidence implicates microtubule stability as a primary driver of disease pathogenesis.

1.3 The function of microtubules and its interaction with tau

Tau plays a role in assembly, stabilization, organization and trafficking of microtubules, which are mainly present in the axon, indicating its role in axonal transport (Cooper GM, 2000; Di Lorenzo, 2024; Qiang et al., 2018; Terwel et al., 2002). Microtubules are a critical component of cytoskeleton, which determines cell shape and have a role in axonal transport. They are composed of tubulin, a globular protein. Tubulin consists of α- and β-tubulin dimers that can polymerize and form protofilaments, which assemble into microtubules (Cooper GM, 2000). The tubulin dimers are also able to depolymerize, which causes the disassembly of microtubules (Mitchison & Kirschner, 1984). The polymerization of tubulin is regulated by guanosine triphosphate (GTP) bound to β-tubulin. GTP hydrolysis into guanosine diphosphate (GDP) can weaken the interaction between tubulin and adjacent molecules. This promotes depolymerization, which allows for a cycle of shrinkage and growth, called dynamic instability (figure 3) (Horio & Murata, 2014; Mitchison & Kirschner, 1984). This dynamic behavior can be regulated by microtubule-associated proteins, either increasing or decreasing microtubule stability (Dehmelt & Halpain, 2004; Di Lorenzo, 2024).

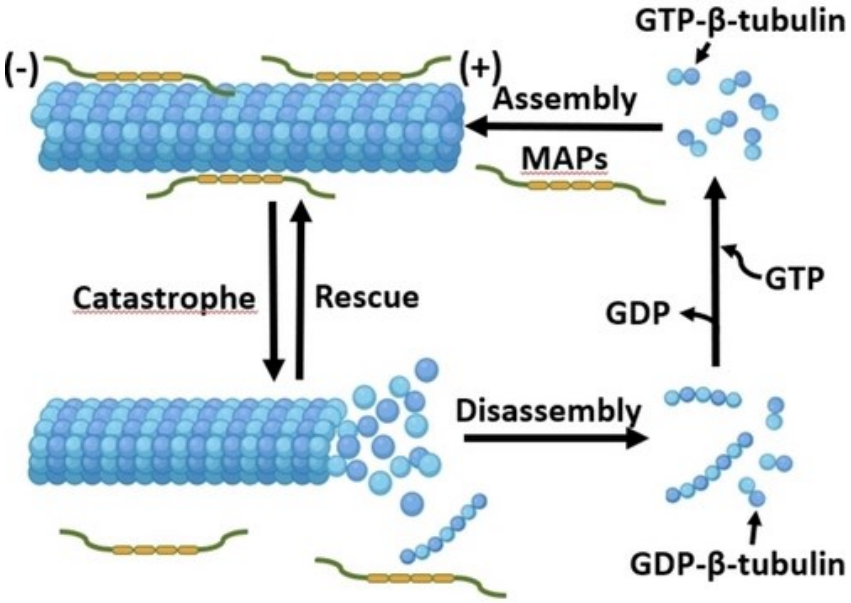

Figure 3: Microtubules undergo polymerization and depolymerization, which allows for the assembly and the disassembly of the microtubules, respectively. This process is called dynamic instability and is needed for physiological functioning. GTP hydrolysis into GDP can promote depolymerization due to weakening of interaction between tubulin (blue) and adjacent molecules. The microtubule-associated molecules (green) can further regulate this dynamic instability by binding microtubules with their microtubule-binding domains (orange) (Di Lorenzo, 2024). Abbreviations: GDP: guanosine diphosphate, GTP: guanosine triphosphate

The function and the stability of tubulin is determined by the tubulin code. The tubulin code consists of the possible different isotypes of tubulin, α- and β-tubulin, which form the microtubules (Verhey & Gaertig, 2007). Tubulin isotypes are transcribed by alternative tubulin genes, which differ between species (Janke & Magiera, 2020). Humans have six α-tubulin and seven β-tubulin isoforms (Sullivan, 1988). Different post-translational modifications are also part of the tubulin code (Verhey & Gaertig, 2007) which are common across many proteins like acetylation, phosphorylation etc. Most of these post-translational modifications on tubulin happen on the C-terminal tail and are specifically abundant in neurons (Janke & Magiera, 2020; Sullivan, 1988).

Two post-translational modifications have been indicated to be important for the stability of microtubules, namely tyrosination and acetylation. When tubulin is incorporated into the microtubules, it is bound to tyrosine in the C-terminal (figure 4). Tyrosination of tubulin is a marker for dynamic tubulin which still undergoes cycles of growth and shrinkage. The tubulin can also be detyrosinated and undergo acetylation and polyglutamylation (figure 4). Acetylation is a unique post-translational modification due to the fact that this does not happen on the C-terminal tail but on lysine 40, located inside the lumen of the microtubules (Soppina et al., 2012). These post-translational modifications of tubulin are often induced after polymerization. Although evidence on whether

acetylation consistently affects microtubule stability is still inconclusive, acetylation has been widely used as marker for stable microtubules in various studies (Katrukha et al., 2021). This is because acetylation appears to protect microtubules from mechanical ageing. This takes place after repetitive cycles of bending. When tubulin is acetylated at lysine 40, they could be less susceptible to breaking during these repetitive cycles (Portran et al., 2017). Stable microtubules are also characterized by an accumulation of detyrosinated tubulin, alongside acetylated tubulin (Portran et al., 2017). There seems to be an unequal distribution of the acetylation and tyrosination along the axons. Acetylation is present along the whole axon but less at the growing end of the axon, while tyrosination is more dominant in the growing end of the axon (Ahmad et al., 1993). In the dendrites, an opposite distribution can be found, namely acetylated in the centre of the dendrite and tyrosinated in periphery of the dendrites. These differences could indicate distinct types of transport (Tas et al., 2017).

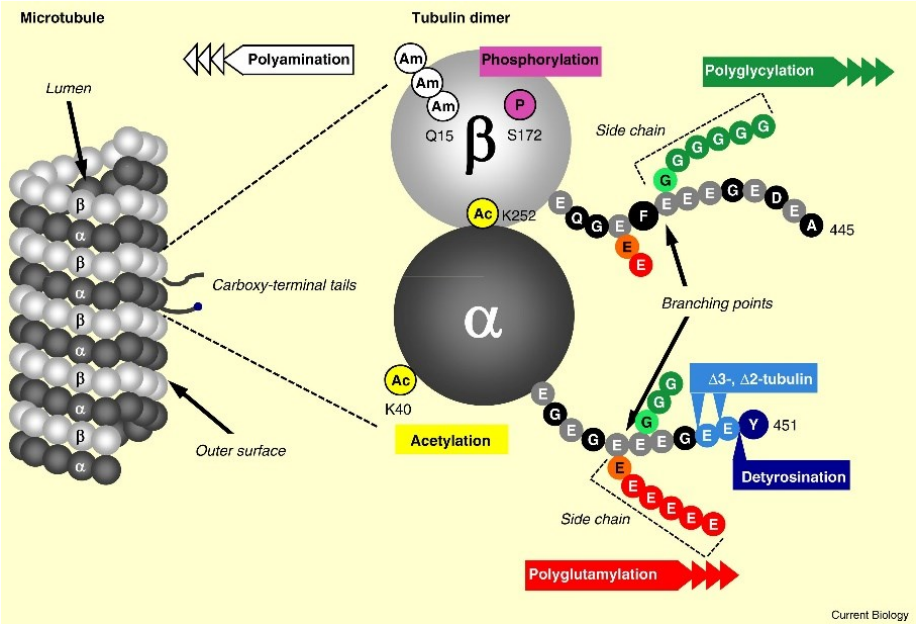

Figure 4: The tubulin code has a clear role in the determination of the stability of microtubules. This code consists of the isotype of the tubulin itself, which can be divided into α- and β-tubulin isotypes. Besides the isotypes, the post-translational modifications of the tubulin are also an important determinant of the stability of the microtubules. Many post-translational modifications are possible of which tyrosination/detyrosination (dark blue) and acetylation (yellow) are two important ones with a role in stability. Tyrosination is a marker of dynamic microtubules and takes place on the C-terminal tail. Acetylation is a marker of stable microtubules and is one of the only post-translational modifications which takes place in the core of the microtubule itself, more specifically on lysine 40 (K40) (Magiera & Janke, 2014).

Tau can interact directly with the microtubules which might influence its stability. The microtubule-binding repeats have four repeated motifs, all separated by flanking regions. The repeated motifs and flanking regions provide the primary structure of the tau protein, allowing it to bind and stabilize the microtubules (T. Guo et al., 2017). The 4R tau protein isoforms have one additional repeat domain, which could be responsible for their higher affinity for microtubules compared to 3R tau isoforms (Goedert & Jakes, 1990). However, these isoforms are also more susceptible for post-translational modifications which might impact its interaction with tubulin (Hanger et al., 2009; Noble et al., 2013). Tau proteins can bind to the C-terminal tail of tubulin, located on the exterior of microtubules, with their microtubule-binding repeats. Upon binding, tau proteins do not alter the structure of microtubules but simply stabilizes them. The first layer of tau proteins is barely visible on the outside of the microtubules which could indicate that tau retains its naturally unfolded structure upon binding. When tau is present in a higher density, they could form a fuzzy coat surrounding the exterior of the microtubules (Santarella et al., 2004).

The exact mechanism by which tau proteins stabilize microtubules is still largely unknown. There are multiple possibilities in which tau could interact with protofilaments, leading to stabilization. Tau could stabilize microtubules by laterally crosslinking the protofilaments of which the microtubules consist of. A second option could be that lateral interactions between protofilaments themselves could be strengthened by tau-tau interactions which could occur between longitudinally bound tau. It might also be possible that different interactions between tau and microtubules could facilitate distinct functions of the microtubules (Duan et al., 2017). Later, a new hypothesis of the role of tau proteins has been brought forward. Tau might promote the elongation of labile domains of axonal microtubules by binding monomeric tubulin subunits. This allows for the assembly and stability of microtubules and enables the rapid microtubule dynamics, possibly playing a role in their stabilization (Qiang et al., 2018).

1.4 The function of mitochondria and their interaction with tau

Mitochondria are responsible for the energy supply of cells. The determining step of adenosine triphosphate (ATP) production within mitochondria is the oxidative phosphorylation (OXPHOS). This biochemical pathway requires the electron transport chain (ETC) complexes (Xu et al., 2020). The ATP synthesis consists of two main parts, which are the generation of the proton gradient by the respiratory chain complexes I-IV and the ATP synthesis by complex V (figure 5) (Chan, 2006). OXPHOS is especially important for the ATP production in neurons since they are not able to switch to glycolysis when OXPHOS is disrupted (Knott et al., 2008). The energy stored in the electrochemical gradient, as a result of the oxidation of nicotinamide adenine dinucleotide (NADH) and succinate, is used by the ATP synthase complex V to produce ATP (Xu et al., 2020).

Each complex plays a crucial role in oxidative phosphorylation. Complex I is a large membrane protein with a molecular weight of almost 1 MDa. It has an L shape with a hydrophobic arm, embedded into the inner mitochondrial membrane and a hydrophilic arm, embedded in the matrix (Hofhaus et al., 1991; Wirth et al., 2016). Complex I is responsible for the oxidation of NADH to NAD+ by flavin mononucleotide to release a pair of electrons. These electrons are transferred by eight Fe-S clusters to ubiquinone (Wikström, 1984). Complex I is also responsible for most of the production of reactive oxygen species (ROS) (Kussmaul & Hirst, 2006).

Complex II consist of four subunits which are arranged in a head-to-tail manner. The head is hydrophilic and consist of succinate dehydrogenase complex flavoprotein subunit A and succinate dehydrogenase complex iron-sulfur subunit B, both located in the matrix. The hydrophobic subunits, succinate dehydrogenase complex subunit C and succinate dehydrogenase complex subunit D, are localized within the inner mitochondrial membrane. Complex II oxidizes succinate to fumarate which allows for the release of electrons that are transferred to ubiquinone via flavin adenine dinucleotide (FAD) and three Fe-S clusters (Sun et al., 2005).

Complex III is a symmetrical dimer which has three core subunits: cytochrome b, cytochrome c, and iron-sulphur protein iron-sulfur protein with a Fe-S cluster. The complex transfers two electrons from ubiquinol to cytochrome c by using a Q-cycle mechanism (Xia et al., 1997; Xu et al., 2020).

Complex IV is composed of 14 different subunits and interacts with complex I. Four electrons from cytochrome c are moved to the terminal electron acceptor O2 which is made possible by the two heme groups and the two binuclear copper centres (Xu et al., 2020).

The last complex involved in OXPHOS is complex V, which is responsible for the ATP synthase itself. It consists of F0, the motor powered by the protons that flow across the membrane, and F1, the motor that generates ATP, located within the mitochondrial matrix (Srivastava et al., 2018).

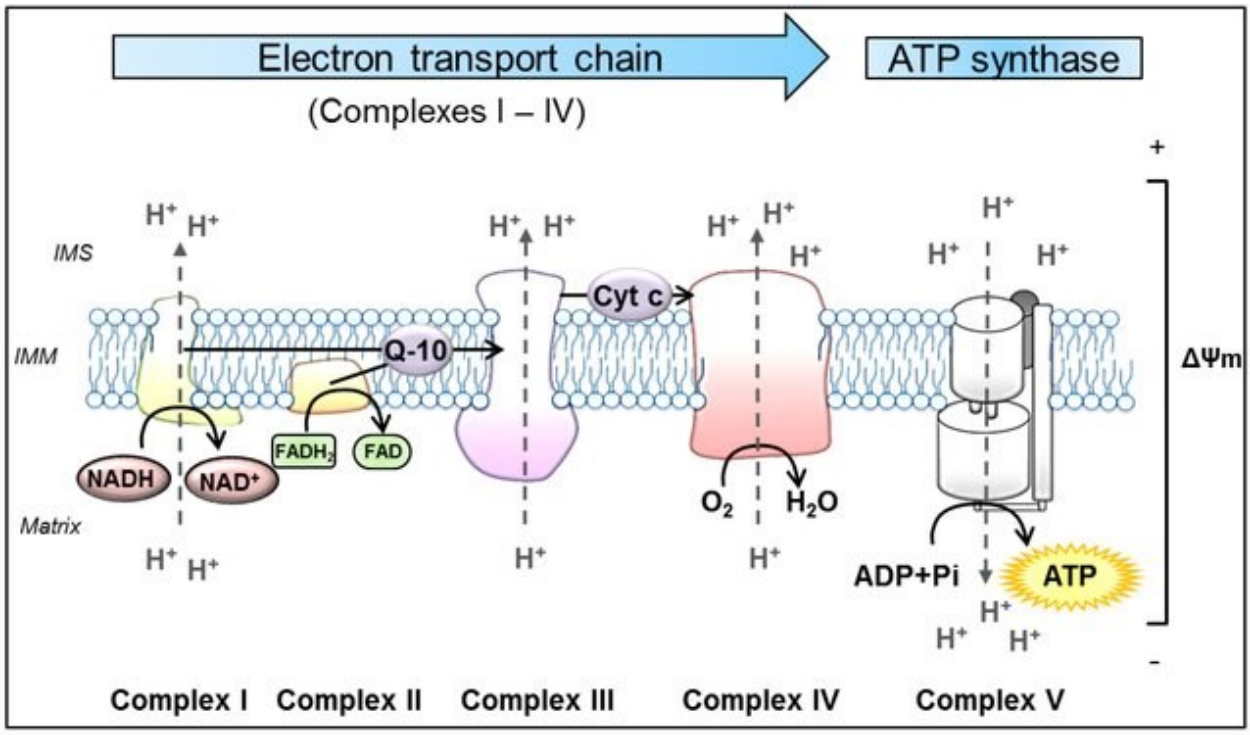

Figure 5: Oxidative phosphorylation within the mitochondria is regulated by five complexes. Complex I-IV are responsible for the formation of the proton gradient across the inner mitochondrial membrane. Complex V uses this proton gradient for ATP production which is used by the neurons as an energy source (Szabo et al., 2020). Abbreviations: ADP: adenosine diphosphate, ATP: adenosine triphosphate, FAD(H2): flavin adenine dinucleotide, IMS: intermembrane space, IMM: inner mitochondrial membrane, NAD(H): nicotinamide adenine dinucleotide, Δψm: mitochondrial membrane potential

There is an abundance of mitochondria within the axons of the neurons which could be an indication of the high energy need within these regions. This is mainly for neurons that are actively participating in synaptic transmission. The cell can tolerate dysfunctional mitochondria to a certain extent, due to the healthy mitochondria compensating for them. However, when the number of dysfunctional mitochondria due to pathogenic mitochondrial DNA reaches a certain threshold, which is tissue-specific, it could become pathogenic. For brain tissue, this bioenergetic threshold is quite low since neurons depend heavily on the oxidative respiratory function (Chan, 2006; Hayashi et al., 1991).

Besides the disrupted ATP production, a dysfunction of the OXPHOS could lead to reactive oxygen species or oxidative stress. In mitochondria, the production of ROS, produced by the electron transport chain, is coupled to the production of ATP, produced by complex V. However, the production of ROS is normally limited. A dysfunction in mitochondria, or in the ETC specifically, could cause an increase in oxidative stress which is toxic to the cell. Elevated oxidative stress markers have been indicated in patients with several neurodegenerative diseases, making them a potential crucial factor in their neuropathogenesis (Alavi Naini & Soussi-Yanicostas, 2015). Oxidative stress could potentially be an early marker for tauopathies like FTD.

Tau has been shown to have a role in maintaining the functionality of the mitochondria. They can do this in several ways. First, mitochondria are produced in the cell body, so they need to be trafficked along microtubules to the synaptic endings. Tau plays a role in transport of mitochondria due to their ability to stabilize tubulin (Schwarz, 2013). Post-translational modifications could interfere with the physiological interaction between tau and microtubules, of which hyperphosphorylation is the most studied (Mietelska-Porowska et al., 2014). Kinesins are responsible for anterograde axonal transport, while dynein is responsible for retrograde axonal transport. Tau participates in both types of transport, affecting kinesin and dynein (Dixit et al., 2008; Duncan & Goldstein, 2006). When transport is impaired, the number of mitochondria at synapses is reduced (Ittner et al., 2008). These synaptic mitochondria are crucial for calcium buffering and the high energy need (Eckert et al., 2014). A possible explanation of how hyperphosphorylated tau disrupts mitochondria trafficking is the extension of its projection domain away from microtubules. This increases the repulsive forces between microtubules, which induce a stronger resistance for mitochondria to move along the microtubules (Shahpasand et al., 2012). Lastly, mitochondrial rho GTPase (Miro) and Milton can be impacted by pathological tau as well. These are proteins that bind the mitochondria and are associated with motor proteins and in that way facilitate mitochondrial trafficking (Guha et al., 2020; X. Guo et al., 2005; Stowers et al., 2002).

Tau proteins and mitochondria can also directly interact and impact each other in different ways. First of all, certain mutations in the tau protein can affect the different complexes involved in OXPHOS. Studies have shown that there is a correlation between the overexpression of mutant tau and the increase of oxidative stress markers and sensitivity to oxidant molecules. This could impact the growth of neurites which could reduce the neuronal connection and in that way the network complexity (Alavi Naini & Soussi-Yanicostas, 2015; Stamer et al., 2002). The accumulation of hyperphosphorylated tau has been shown to impair complex I and complex V activity, causing mitochondrial dysfunction and high levels of ROS (David et al., 2005; Guha et al., 2020). A study on human induced pluripotent stem cells (hiPSC) with an IVS10+16 mutation showed hyperpolarized mitochondria, inhibition of complex I respiration, decreased ATP production and oxidative stress (Esteras et al., 2017). The relationship between oxidative stress and the tau aggregation is not a one-way street but a vicious cycle, where both can influence each other to cause an increase in phosphorylation and dysfunctional mitochondria. It has been shown that the elevated levels of oxidative stress can induce an increase in tau hyperphosphorylation and the aggregation of tau in vitro (Gómez‐Ramos et al., 2003; Pérez et al., 2000). Oxidative stress might be able to activate p38 mitogen-activated protein kinase (MAPK). This is a kinase that has been shown to be capable of phosphorylating tau in vitro (Goedert et al., 1997). When studying hippocampal and cortical brain regions of Alzheimer disease patients, activated p38 was exclusively found within NFTs. These results might suggest the role of p38 MAPK in phosphorylation of tau and formation of tau tangles in vivo (Zhu et al., 2000).

Tau could also induce bioenergetic deficits. It could downregulate the subunits of mitochondrial complexes I and V (David et al., 2005). Deficits in complex I would impact the mitochondrial membrane potential. Complex V is responsible for the ATP production, as a result of the mitochondrial membrane potential. Impairment of either complexes will impair OXPHOS and result in a decrease in ATP production (Srivastava et al., 2018; Wikström, 1984). Interactions between wild-type tau and proteins on the inner mitochondrial membrane, for example complex I, III, IV and ATPase have been shown to be diminished in FTD mutations in iPSC models. In V337M neurons, this was associated with altered mitochondrial bioenergetics with decreased coupling efficiency, resulting in decreased ability of maintaining ATP levels under energetic stress. P301L mutant tau results in impaired ATP synthesis and increased susceptibility to oxidative stress (David et al., 2005; Schulz et al., 2012; Tracy et al., 2022).

Additionally, pathological tau could affect mitochondrial dynamics. It could cause the elongation of mitochondrial network, which will have difficulties in axonal transport (DuBoff et al., 2012; Szabo et al., 2020). A plausible reason for this elongation could be the mislocalization of dynamin-1-like protein (Drp1), due to tau increasing the F-actin stabilization and in its turn disturbing the physiological association of Drp1 and mitochondria (Bardai et al., 2018). In Alzheimer's disease models, it has been shown that phosphorylated tau interacts with Drp1. This interaction was accompanied by increased GTPase activity resulting in increased fragmentation of mitochondria, due to its role in mitochondrial fission (Manczak & Reddy, 2012). However, a drosophila model with pseudo-hyperphosphorylated tau showed increased fusion and decreased fission in comparison to wild-type tau and FTD mutation. This through the stabilization of actin which inhibits its association with Drp1 (DuBoff et al., 2012). The disruption in both fusion and fission processes lead to mitochondrial dysfunction (Guha et al., 2020).

In normal circumstances, these dysfunctional mitochondria would be removed by mitophagy. Dysfunctional mitochondria are recognized by a phagophore due to a depolarization of the membrane potential of mitochondria. This forms a mitophagosome that fuses with the lysosome to degrade the mitochondria. There have been studies indicating that pathological tau might impact the mitophagy in tauopathies. The exact mechanism used by pathological tau to impair mitophagy is still unclear. However, this could lead to an accumulation of dysfunctional mitochondria, causing an increase in ROS production and decrease in ATP production (Guha et al., 2020).

1.5 Introducing 4R tau into iPSCs

Both synonymous and missense *MAPT* mutations have been found to be associated with FTD. These mutations can influence the biology of tau in three diverse ways. Firstly, it can reduce the ability to bind to microtubules (Hong, 1998). Secondly, it can alter the tau splicing which will alter the ratio of 3R:4R in the brain (Hutton et al., 1998). Lastly, it could also increase the formation of tangles when polyanions are present in vitro (Friedhoff et al., 1998).

IPSCs naturally show low levels of 4R tau. However, increased levels of 4R tau, disrupting the 3R:4R ratio, has been shown to be important in several primary tauopathies including FTD (Rösler et al., 2019). This means that iPSC lines need to be adjusted to express higher levels of 4R tau, so that its involvement in primary tauopathies can be investigated. Bowles et al. (2024) generated iPSC lines with mutations in the *MAPT* gene at position 305, based on mutations found in patients with FTD, as well as isogenic corrected controls. This mutation causes familial FTD due to a high expression of 4R tau (Bowles et al., 2024).

In wild-type tau, position 305 in exon 10 is a serine (AGU). By adding a single point mutation within this position, the serine can be changed to asparagine (AAU). By mutating AGU into AUU, an isoleucine is translated instead of a serine. Both S305N and S305I, respectively, are missense mutations that change the RNA hairpin-loop structure. The RNA hairpin-loop structure is responsible for the alternative splicing of exon 10 and so regulates the difference between 3R (exclusion) and 4R (inclusion) (figure 6).

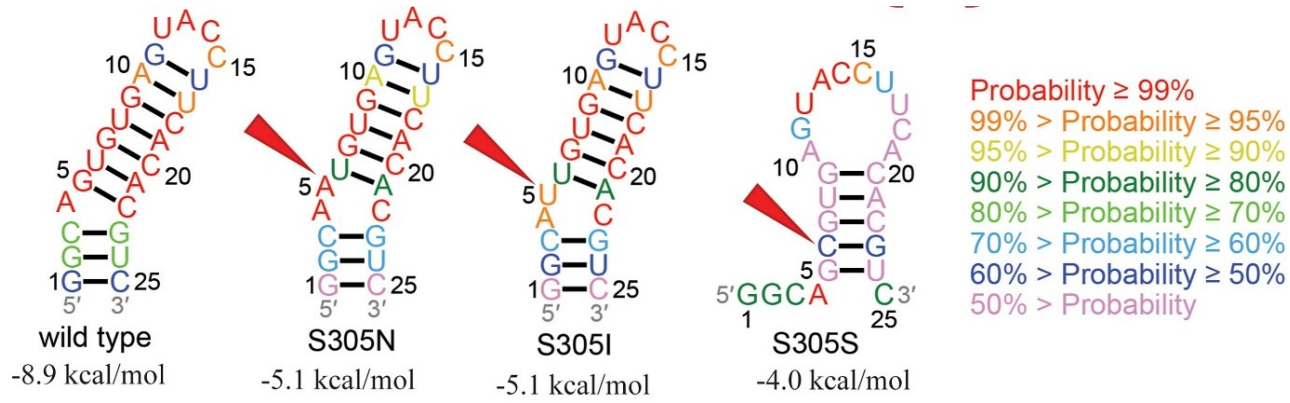

Figure 6: Both missense (S305N and S305I) and synonymous (S305S) mutations at position 305 can impact the RNA hairpin-loop structure of MAPT gene. This structure is important in the alternative splicing of exon 10 responsible for the formation of 3R tau or 4R tau. By introducing these mutations, the ratio of 3R:4R can be modified, introducing an increase of mutant and wild-type 4R tau, respectively. The colours indicate the probability of base-paired and single-stranded nucleotides in the sequences (Bowles et al., 2024).

The S305N *MAPT* gene mutation causes a reduction in thermodynamic stability of the RNA hairpin-loop structure, causing an increase in alternative splicing of exon 10 (Hasegawa et al., 1999; Varani et al., 1999). S305N has been shown to have the highest increase in mutated 4R tau levels, which could be explained by the highest destabilization (Bowles et al., 2024; Chen et al., 2019). S305I also causes an increase in 4R isoform due to effect of the mutation on the stability of RNA hairpin-loop structure (Kovacs et al., 2008).

S305S is a synonymous mutation. This mutation increases the inclusion of exon 10 by a single point mutation, AGU to AGC, resulting in the same amino acid. Even though the mutation is silent on the level of the amino acids, it is believed to destabilize the RNA hairpin-loop structure, which could still increase the level of wild-type 4R tau (figure 6) (Stanford et al., 2000).

IVS10+16 mutation in the *MAPT* gene has been shown to express elevated levels of wild-type 4R, which can be a control for the comparison with mutated 4R tau (Verheyen et al., 2018). The IVS10+16 mutation is within the intronic region, 16 nucleotides downstream from the beginning of intron 10. This mutation also impacts the exon 10 – intron 10 RNA hairpin structure (Bowles et al., 2024).

Both IVS10+16 *MAPT* mutations and S305S *MAPT* mutations induce an increase in wild-type 4R tau. This causes wild-type 4R tau to be present in early stages of the development, in which it normally is not present (Goedert et al., 1989; Trabzuni et al., 2012). Both mutations result in a similar age of disease onset (Hutton et al., 1998). However, the IVS10+16 iPSCs show inclusion of exon 10 in a progressive manner within several months (Sposito et al., 2015). For S305S, this is not a progressive increase, but these iPSCs show an early and sustained inclusion of exon 10 (Bowles et al., 2024).

When studying the atrophy between missense *MAPT* gene mutations and synonymous *MAPT* gene mutations, they both show gray matter loss in the medial temporal cortex. The pattern of this atrophy is very similar between S305N and IVS10+16 *MAPT* gene mutations (Whitwell et al., 2009). This would indicate that both have similar pathogenesis. However, they might impact different mechanisms early in the development of FTD, both leading to similar patterns of atrophy. Previous comparisons of different splicing mutations in *MAPT* gene, resulting in mutated and wild-type 4R tau protein, suggest differential effects on OXPHOS and gene expression regulation. Synonymous mutations, more specifically S305S *MAPT* gene mutation, showed impaired OXPHOS, implying mitochondrial dysfunction. Not only OXPHOS but also non-mitochondrial respiration was downregulated. On the other hand, missense mutations showed upregulated respiration, which could reflect an increase in ROS production (Bowles et al., 2024). However, it is still unclear if and/or how these different mutations act differently in neurons.

2. Aim of work

The work described in this thesis was carried out at Bowles lab, part of UK-DRI at University of Edinburgh.

FTD is a heterogenous group of neurocognitive disorders. Even though tau tangles have been found in FTD patients and have been shown to be involved in the disease development, the exact neuropathogenesis and mechanisms causing the disease are still largely unknown. The heterogeneity of the disease indicates that the mechanisms involved in the development of FTD might differ in different patients. For this thesis, we focused on FTD-tau, involved in approximately 50% of the FTD patients, with a specific focus on missense and synonymous mutations in the *MAPT* gene.

Seeing as different splicing mutations result in mutant or wild-type 4R tau proteins (Bowles et al., 2024), we hypothesised that each mutation type will differentially affect microtubule stability and mitochondrial function. To address this, we aimed to:

1. Characterize the impact on tau levels and phosphorylation of tau
2. Characterize the impact on mitochondrial mass and mitochondrial functionality
3. Assess the impact on microtubules dynamics, in regard to the ratio between unstable and stable tubulin

These aims were completed in an iPSC organoid model, in order to explore both temporal changes and genotype-specific effects potentially leading to FTD by comparing mutations and wild-type models over time.

3. Materials and Methods

3.1 Generation and Differentiation of Organoid Cultures

iPSCs of four different donors have been used, of which ten lines of organoids were made (table 1) obtained from the Tau Consortium Collection. The iPSCs were derived from peripheral blood mononuclear cells from individuals with S305N mutations and lymphoblastoid cell lines from an S305S mutation carrier. The cells were reprogrammed to iPSCs using Sendai-virus-mediated gene transfer of *OCT4*, *SOX2, KFL4* and *c-MYC* at the Icahn School of Medicine at Mount Sinai Stem Cell core facility. Isogenic corrected wild-type (WT) controls and homozygous mutations were generated using CRISPR-Cas9 genome editing. Both the missense and synonymous mutation organoid lines showed an increase in expression of the 0N4R tau isoform. The generation and differentiation of organoid cultures was performed by the lab for me to process (Bowles et al., 2024).

Table 1: iPSCs of four donors are used to make ten lines of organoids. The first five lines are wild-type combined with their missense mutation. The last five lines are wild-type combined with their synonymous mutation (Bowles et al., 2024).

Sample name	**Parent ID**	**Isogenic genotype**	**Type of mutation**
NWBB7	300.12	WT/WT	NA
NW1C7	300.12	S305N/WT	Missense
HCB8	300.12	S305N/S305N	Missense
S2A3	F13505.1	WT/WT	NA
NDG11	F13505.1	S305N/WT	Missense
WAC11	GP1.1	WT/WT	NA
SW1D8	GP1.1	S305S/WT	Synonymous
SH1G8	GP1.1	S305S/S305S	Synonymous
DO1	GIH-36-C2	WT/WT	NA
EO4	GIH-36-C2	IVS10+16/WT	Synonymous

3.2 Protein lysates

To prepare protein lysates, radioimmunoprecipitation assay (RIPA) buffer was made with 1x protease/phosphatase inhibitor of which 200µl was added to each organoid sample. Each sample consist typically of three organoids. The samples were briefly sonicated to dissociate tissue and lyse cells and centrifuged at 13.000 x g for ten minutes at 4°C to pellet the debris. The volume of sample needed was determined with Bicinchoninic Acid Assay (BCA) using the Thermo BCA Protein Assay Kit #23225. Standards were prepared using bovine serum albumin (BSA) following table 2. The standards and samples were pipetted in duplicate into flat-bottomed clear 96-well plate (5µl). To each well, 200µl BCA solution, consisting of 1:50 dilution of solution A to solution B, was added. The sealed plate was incubated at 37°C for 20-30 minutes and read on the spectrophotometer at 565 nm.

Table 2: Dilution series used as standard for the BCA

Vial	**Water**	**Source of BSA**	**Concentration**
A	0 µl	300 µl of stock	1000 µg/ml
B	125 µl	375 µl of stock	2000 µg/ml
C	325 µl	325 µl of stock	1500 µg/ml
D	175 µl	175 µl of B	1000 µg/ml
E	325 µl	325 µl of C	750 µg/ml
F	325 µl	325 µl of E	500 µg/ml
G	325 µl	325 µ of F	250 µg/ml
H	400 µl	100 µl of G	125 µg/ml
I	400 µl	0 µl	0 µg/ml

3.3 Mitochondria isolation

For the preparation of mitochondria isolates, three organoids per sample were dissociated on ice using a dounce homogenizer, with five strokes of pestle B. The Mitochondria Isolation Kit for Cultured Cells from ThermoFisher was used for the isolation. BSA was added to reagent A to make 4mg/ml followed by addition of protease inhibitor to isolation reagents A and C. The samples were washed two times with phosphate-buffered saline (PBS) and lastly 800µl of PBS was added. This was centrifuged for three minutes at 1000 x g at 4°C. The supernatant was discarded and the pellet was resuspended in 800µl BSA/reagent A, followed by vortexing. This was incubated on ice for exactly two minutes. After those two minutes, 800µl of isolation reagent B was added and the samples were vortexed again. This was incubated on ice for five minutes, vortexing at maximum speed every minute. Next, 800µl of isolation reagent C was added and inverted to mix, followed by centrifugation at 700 x g for ten minutes at 4°C. The pellet was discarded and the supernatant was moved to a new tube and centrifuged at 3000 x g for 15 minutes at 4°C. The supernatant was kept as the cytosolic fraction and the pellet was washed with 500µl wash buffer. This was centrifuged for five minutes at 12.000 x g, the supernatant was discarded and the pellet containing mitochondria was kept. Lastly, 50µl of 2% 3-[(3-cholamidopropyl)dimethylammonio]-1-propanesulfonate (CHAPS) in tris-buffered saline (TBS) was added to the pellet and vortexed for one minute. This was centrifuged at high speed for two minutes to pellet, in which the supernatant contained the soluble proteins.

3.4 Sodium dodecylsulfate – polyacrylamide gel (SDS-PAGE) electrophoresis

The sample was diluted in water and combined with lithium dodecyl sulphate and reducing agent for denaturation at 70°C for ten minutes. If detection of OXPHOS was needed later, 37°C for 30 min was used for denaturation. The volume of sample diluted depended on the BCA results for protein lysates and was 5-10µl for mitochondrial isolates. As running gel, Bolt 4-12%, Bis-Tris Plus Wedgewell gel from Invitrogen (Thermo Fisher Scientific) was used, which was loaded with SeeBlue Plus2 prestained standard ladder (Thermo Fisher Scientific), tau isoform ladder (rPeptide) and the samples. Samples underwent electrophoresis for 22 min at 220V, followed by blotting with the iBLOT2 from Thermo Fisher Scientific using an iBlot2 nitrocellulose stack.

3.5 Western blot

The nitrocellulose membranes were first blocked with a 5% milk in PBST solution (1x phosphate buffered saline with 0,1% tween). The membranes were then stained with primary antibody solution overnight at 4°C. The primary antibodies used were OXPHOS cocktail (Abcam), paired helical filament-1 antibody (PHF1), which stains p-tau at ser396 and ser404, and DA9 (both kind gifts from Profs. Peter Davies and Jeremy Koppel), which stains total tau (epitope at amino acid 102-140) at a concentration of 1:500 and the housekeeping gene glyceraldehyde 3-phosphate dehydrogenase (GAPDH) (Cell Signalling Technologies) at a concentration of 1:10,000 for organoids lysates or the housekeeping gene translocase of outer mitochondrial membrane 40 (TOMM40) (Proteintech) at a concentration of 1:500 for mitochondria isolates. Before adding the secondary antibody solution, membranes were washed three times in PBST. The secondary antibodies used were either goat-anti-rabbit, bound to horseradish peroxidase (HRP) (Invitrogen, Thermo Fisher scientific) for visualization with enhanced chemiluminescence (ECL) or donkey-anti-mouse-800CW and goat-anti-rabbit-680RD (LI-COR) for visualization by fluorescence. After incubation of one hour at room temperature, membranes were washed three times with PBST.

Thermo Fisher SuperSignal West Pico PLUS chemiluminescent Substrate was used for HRP detection and membranes were imaged using X-ray film on the MI-5 X-ray film processor. Membranes were imaged on the LI-COR Odyssey CLx imager in case of visualization by fluorescence. Quantification was performed by using densitometry in ImageJ for both imaging approaches. Protein levels were normalized to GAPDH (organoid lysates) or TOMM40 (mitochondria isolates) and the mutated lines are then normalized to their wild-type.

After detection of a certain protein, membranes were stripped with Restore PLUS Western Blot Stripping Buffer from Thermo Fisher Scientific (ECL) or Restore Fluorescent Western Blot Stripping Buffer from Thermo Fisher Scientific (fluorescence) to stain the membrane for the next protein. Membranes were incubated with the stripping buffer for 15 minutes. The stripping buffer was removed and PBS was added to the membrane for five minutes. After five minutes, membranes were blocked again with 5% milk in PBST solution and restained according to protocol mentioned above.

3.6 Polymerase Chain Reaction (PCR)

PCR combined with quantification was used to determine the ratio between mitochondrial and nuclear DNA. This was done by performing a PCR with a primer pair for mitochondrial DNA and a primer pair for nuclear DNA. One organoid per line was used for DNA extraction with the DNeasy Blood and Tissue Kit from Qiagen. The organoid was suspended in 200µl PBS, 20µl Proteinase K and 200µl Buffer AL. This was vortexed until the organoid dissolved. After vortexing, 200µl 100% ethanol was added to the samples and vortexed again. The mixture was pipetted into DNeasy Mini Spin Column placed in a 2ml collection tube. The column within the collection tube was centrifuged at 6000 x g for one minute and the flow-through and collection tube was discarded. The column was placed in a new collection tube and 500µl AW1 buffer was added. This was centrifuged again at 6000 x g for one minute. The flow through and collection tube were discarded and the column was placed in a new collection tube. In the column, 500µl of AW2 buffer was added and this was centrifuged for three minutes at 20.000 x g. Again, the flow through and the collection tube were discarded and the column was placed in a 1.5ml microcentrifuge tube. DNA was eluted by using 200µl of AE buffer. This was incubated for one minute at room temperature and afterwards centrifuged for one minute at 6000 x g.

For quantification of these DNA samples after DNA extraction, to normalize all samples to have 10ng/µl, the DeNovix DS7+ spectrophotometer was used. AE buffer was used as a blank and 1µl of blank/sample was used for measurement. These dilutions were used for the PCR reaction. A PCR mix of 12.5µl of 2x Phusion Mix with HF buffer (Thermo Fisher Scientific), 1,25µl of 10uM forward primer, 1,25µl of 10uM reverse primer, 7µl of water and 3µl per sample was prepared. This mix was made for both mitochondrial DNA and nuclear DNA for each sample. PCR reaction was performed according to following protocol:

- Lid: 105°C
- Volume: 25 µl
- Initial denaturing: 98°C, 0:30
- Denaturation: 98°C: 0:10
- Annealing: 67°C, 0:30
- Extension: 72°C, 0:30
- Repeat cycle (denaturation – extension) 34x
- Final extension: 72°C, 10:00

The primer sets used for nuclear DNA and mitochondrial DNA were the following:

- Nuclear DNA primers: B2-microglobulin
  Nuclear forward 5'- TGCTGTCTCCATGTTTGATGTATCT -3'
  Nuclear reverse 5'- TCTCTGCTCCCCACCTCTAGT -3'
- Mitochondrial DNA primers: transfer RNA Leu (URR)
  Mitochondrial forward 5'-CACCCAAGAACAGGGTTTGT -3
  Mitochondrial reverse 5'- TGGCCATGGGTATGTTGTTA -3'

The samples were analysed and DNA was quantified using D1000 ScreenTapes on the Agilent Technologies 4200 TapeStation after PCR amplification

3.7 Super-resolution structured illumination microscopy (SIM)

The super-resolution structured illumination microscopy was performed on a Zeiss Elyra 7 to visualize distinct post-translational modifications indicating stability of tubulin. Cryosections of two-months-old, four-months-old and six-months-old organoids were stained with anti-tubulin antibodies to determine the presence of different tubulin structures. All steps were performed in a humidity chamber. First, the sections were permeabilized and blocked with 1% BSA and 0.1% Triton in PBS for 30 minutes. Slides were washed three times with PBS after every step. The sections were stained with primary antibodies anti-Tubulin Tyrosinated (Abcam) and anti-Tubulin Acetylated (Sigma-Aldrich) at a concentration of 1:1000 and anti-Alpha Tubulin antibody (Abcam) at a concentration of 1:500 and incubated overnight at 4°C. After three washes with PBS, secondary antibodies were added and incubated for minimum two hours at room temperature. Secondary antibodies used were goat-anti-rat-488, goat-anti-mouse-647 and donkey-anti-rabbit-568, respectively, at a concentration of 1:100. Lastly, a 4',6-diamidino-2-phenylindole (DAPI) staining (Invitrogen, Thermo Fisher Scientific) was added at a concentration of 1:5000 for ten minutes. Slides were mounted with ProLong Glass mounting media and a coverslip was added.

Images were taken in four channels with a Plan-Apochromat 63x/1.40NA oil objective and captured on a 2560 x 2560 grid and pixel size of 31.3 nm for a field of view (FOV) of 80.14 x 80.14 µm using dual Hamamatsu ORCA-Flash4.0 V3 sCMOS cameras (Hamamatsu Photonics). Lattice-SIM processing was performed with a scaling to min/max of the histograms. ImageJ was used for quantification of acetylated, tyrosinated and total tubulin by measuring fluorescent area for each antibody linked to a fluorophore. No threshold was set for intensity of fluorescence due to SIM processing, but a background subtraction was performed in ImageJ before quantification. Acetylated and tyrosinated tubulin were normalized to total tubulin and the acetylated tubulin, tyrosinated tubulin and the ratio between both of mutated organoid lines were subsequently normalized to their wild-type.

3.8 Flow cytometry

Flow cytometry was performed to detect MitoTracker (mitochondrial mass), MitoSOX (oxidative stress, specifically superoxide) and tetramethylrhodamine, methyl ester (TMRM) (membrane potential) to study mitochondrial health in different mutations over time. This was performed for organoids of two months, four months and six months. Before flow cytometry, the organoids were dissociated using papain. The papain solution was prepared by adding 5ml of Earle's balanced salt solution (EBSS) to the papain. This solution was put in a water bath for ten minutes until the papain was completely dissolved. After this, 250µl of DNase I was added to 5ml of papain solution before starting dissociation. Ovomucoid inhibitor was reconstituted with 32ml EBSS. The organoids were cut into smaller pieces with a scalpel blade and transferred into a 1.5ml tube. The medium was then aspirated and 1ml PBS was added to let the organoid pieces settle. After this, the PBS was removed again and 600-750µl of papain solution was added. This was incubated for 30 minutes at 37°C on a heat block with gentle shaking (300 rpm) and triturated 10-15x with a glass Pasteur pipet. After, the samples were incubated for 60 more minutes with trituration every 15 minutes until a single cell suspension was achieved. Following this incubation, 500µl of EBSS, 150µl reconstituted Worthington inhibitor solution and 30µm DNase I solution was added to the dissociated tissue. This was mixed gently and centrifuged at 300 x g for three minutes at room temperature. Cells were resuspended in 300µl ice cold PBS and passed through a 35-micron filter. After filtering, the samples were split into two Eppendorf tubes per sample to add two different labelling mixes.

The first labelling mix consisted of the MitoTracker, MitoSOX and Live/Dead Violet. To make this mix, 74,4µm dimethyl sulphoxide (DMSO) was added to MitoTracker to make 1mM stock. This was diluted in PBS at a concentration of 1:10,000. MitoSOX red was mixed with 13µl DMSO and added to the PBS/MitoTracker mix at a concentration of 1:1000. Lastly, Live/Dead Violet was mixed at a concentration of 1:1000 with 50µl DMSO and added to PBS/MitoTracker/MitoSOX. For the second mixture, TMRM and Live/Dead Violet was added to PBS at a concentration of 1:1000. To each sample, 1ml of labelling mix was added and incubated for 30 minutes at 37°C. These samples were centrifuged for five minutes at 300 x g to pellet the cells. The supernatant was discarded and cells were resuspended in 100µl 0.1% BSA in PBS and transferred to a 96-well V-bottomed plate. Cell analysis took place on the Attune Cytopix and FlowJo was used for the data analysis.

3.9 Statistical analysis

For all tests performed, various sample sizes have been used for different time points due to availability of samples and technical issues in visualization. Samples sizes (n) have been clarified in the relevant figure legends. The different wild-type (four per replicate), missense (three per replicate) and synonymous (three per replicate) mutation organoid lines were grouped per time point for comparison. Comparisons across time and different genotypes were performed using ANOVA test followed by Tukey's multiple comparison test using GraphPad. Potential outliers have been identified and removed by ROUT analysis (Q = 0,1%) in GraphPad.

4. Results

4.1 Total tau was significantly decreased between two months and four months in synonymous MAPT gene mutation organoid lines

To determine if the missense or synonymous mutations impact tau protein abundance or phosphorylation over time, a quantitative analysis of PHF1 (figure 7D), DA9 (figure 7E) and PHF1/DA9 ratio (figure 7F) was performed, following a western blot (figure 7A, 7B, 7C). Visually, the protein levels of PHF1 were similar between mutant and wild-type organoids at two months. In four-months-old organoid lysates, the expression levels of PHF1 were decreased in synonymous mutations, which returned back to levels comparable to the wild-type at six months.

Total tau (DA9) was slightly increased at two months but significantly decreased, according to ANOVA statistical analysis, at four months. At six months, DA9 expression levels in synonymous mutations went back to similar levels compared to the wild-type but was slightly decreased in missense mutations. When comparing the ratio between PHF1 and DA9, relative phosphorylated tau levels remained the same over time in both synonymous and missense *MAPT* gene mutation organoid lysates with a slight increase in missense mutations and a slight decrease in synonymous mutations at two months.

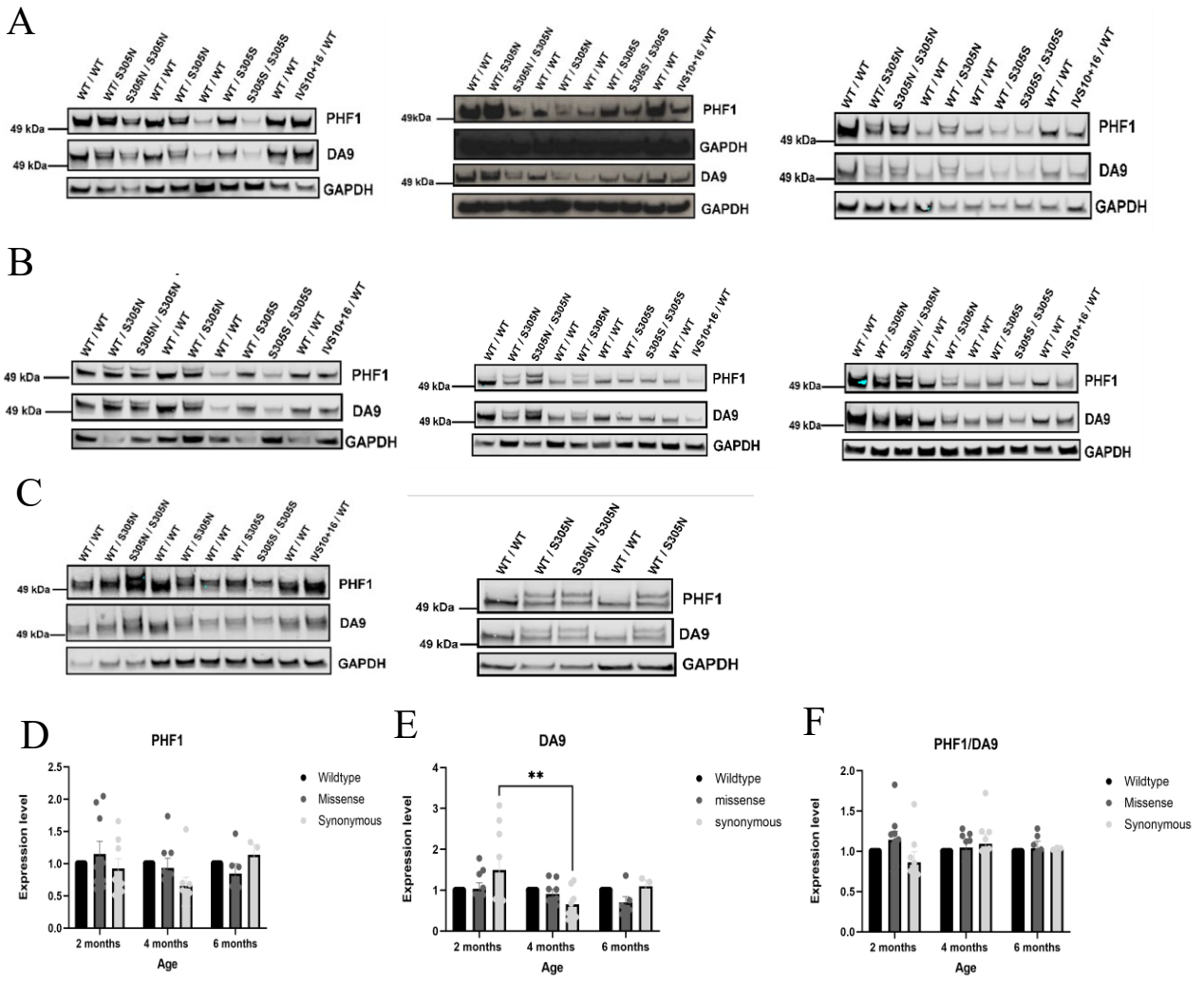

*Figure 7: Visualization of PHF1, DA9 and GAPDH (housekeeping protein) of organoid lysates either by ECL or by fluorescence at A. two months (three replicates), B. four months (three replicates) and C. six months (two replicates for missense mutations and one replicate for synonymous mutations). Quantification of D. PHF1, E. DA9 and F. PHF1/DA9 in wild-type and mutation organoids over time. Error bars indicate SEM. Sample sizes used for the analysis are D. n(2months - missense) = 9, n(2months - synonymous) = 8, n(4months) = 9, n(6months - missense) = 6 and n(6months - synonymous) = 3, E. n(2months) = 9, n(4months) = 9, n(6months - missense) = 6 and n(6months - synonymous) = 3 and F. n(2months - missense) = 9, n(2months - synonymous) = 8, n(4months) = 9, n(6months - missense) = 6 and n(6months - synonymous) = 3. Two-way ANOVA, Tukey's multiple comparisons test. **p < 0.01*

4.2 Complex II was significantly increased at four months in missense mutation organoid lines

Secondly, a quantitative analysis of complex I to V, involved in OXPHOS, was performed over time, following a western blot (figure 8A, 8B, 8C). Due to technical constraints of the antibody mix, not all complexes were visualized and quantified for each timepoint and each mutation.

Expression levels of complex I (figure 8D) and complex V (figure 8F) remained relatively equal across wild-type and different mutations over time. A small increase in complex I was found in missense mutation at two months. For complex II (figure 8E), the expression level was relatively the same between the mutated lines and their wild-type at two months and six months. However, at four months, there was a significant increase, according to ANOVA statistical analysis, of complex II levels in the missense mutations in comparison to their wild-type and the synonymous mutations became visible.

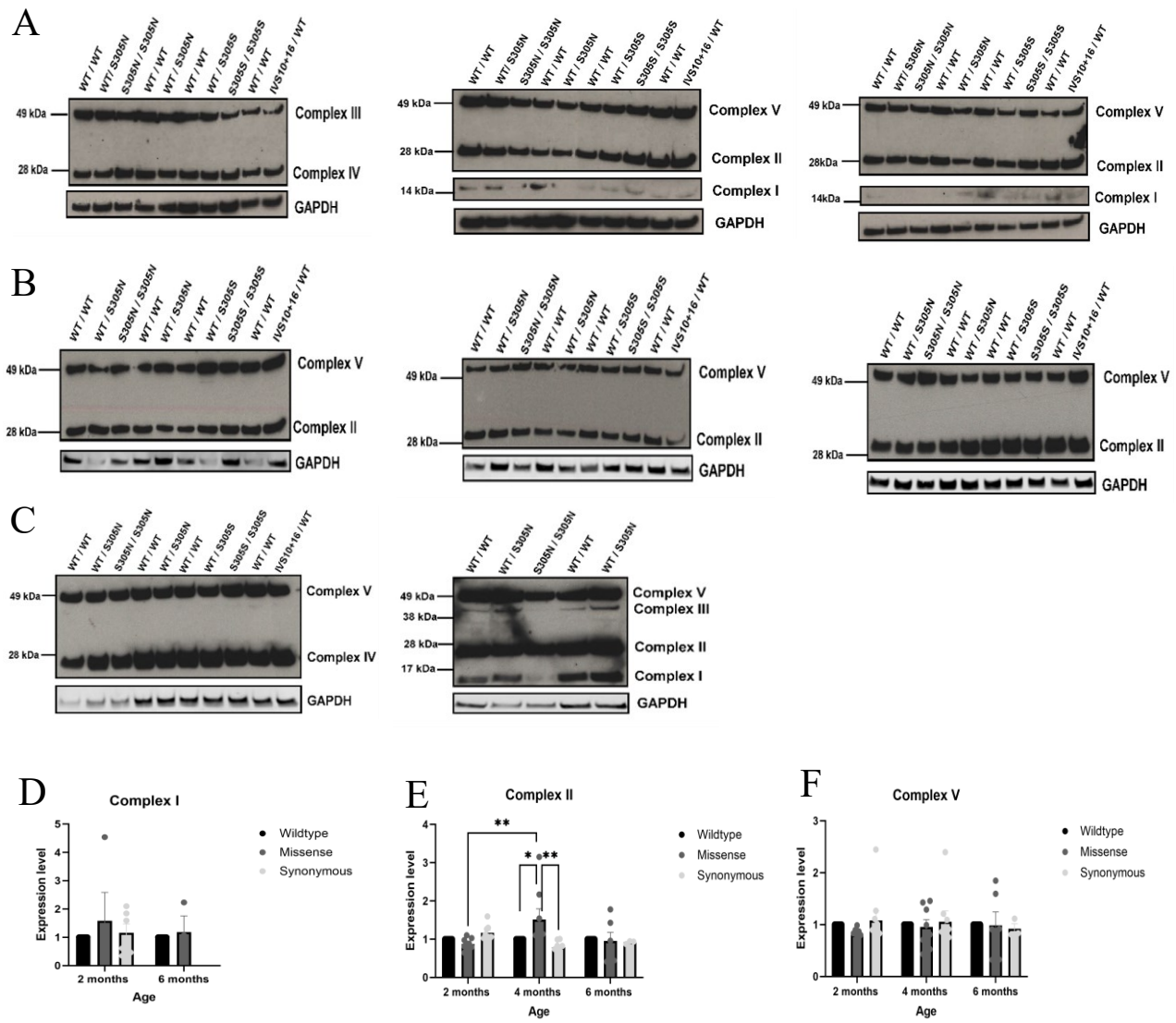

*Figure 8: Visualization of PHF1, DA9 and GAPDH (housekeeping protein) of organoid lysates either by ECL or by fluorescence at A. two months (three replicates), B. four months (three replicates) and C. six months (two replicates for missense mutation and one replicate for synonymous mutation). Quantification of D. complex I, E. complex II and F. complex V in wild-type and both mutation organoids over time. Error bars indicate SEM. Sample sizes used for the analysis are D. n(2months - missense) = 4, n(2months - synonymous) = 6, n(6months - missense) = 3, E. n(2months) = 9, n(4months) = 8, n(6months - missense) = 6, n(6months - synonymous) = 3 F. n(2months) = 9, n(4months) = 8, n(6months - missense) = 6, n(6months - synonymous) = 3. Two-way ANOVA, Tukey's multiple comparisons test. *p < 0.05, **p < 0.01*

4.3 A significant difference of phosphorylated tau, total tau and their ratio was found between wild-type and mutation mitochondrial isolates over time

The quantitative analysis of PHF1 (figure 9D), DA9 (figure 9E) and PHF1/DA9 ratio (figure 9F) over time was performed in mitochondria isolates as well, following a western blot (figure 9A, 9B, 9C). A two-way ANOVA followed by Tukey's multiple comparisons test revealed statistically significant differences between the wild-type and mutants over time.

First of all, there was a significant increase in PHF1 in synonymous mutations over time, which was not seen in missense mutation mitochondrial isolates. Comparing the mutations with their wild-type within time points, a significant increase in PHF1 expression levels in synonymous *MAPT* mutations was found in four months and six months. These expression levels of PHF1 progressively increased over time. At six months, there was a slight decrease of PHF1 expression levels in missense mutation mitochondria isolates compared to the slight increase at two months and four months.

For DA9, a significant difference was found over time in the synonymous mutation as well. The expression levels of DA9 first increased significantly at four months and then decreased again slightly at six months but stayed elevated compared to expression levels at two months. The same pattern in DA9 expression was found in missense mutation mitochondria isolates, with a stronger decrease at six months. Compared to their wild-type within a time point, missense mutation showed increased expression levels of DA9 at four months and synonymous mutation showed increased expression levels at both four months and six months.

To determine the relative expression levels of phosphorylated tau, a ratio between PHF1 and DA9 was calculated. This ratio showed a decrease of relative phosphorylated tau expression levels in both missense and synonymous mutations between two months and four months. These levels increased again to an expression level similar to the wild-type at six months. Comparing relative phosphorylated tau expression levels within time points indicated a significant increase in synonymous mutations at two months and a significant decrease in missense mutations at four months.

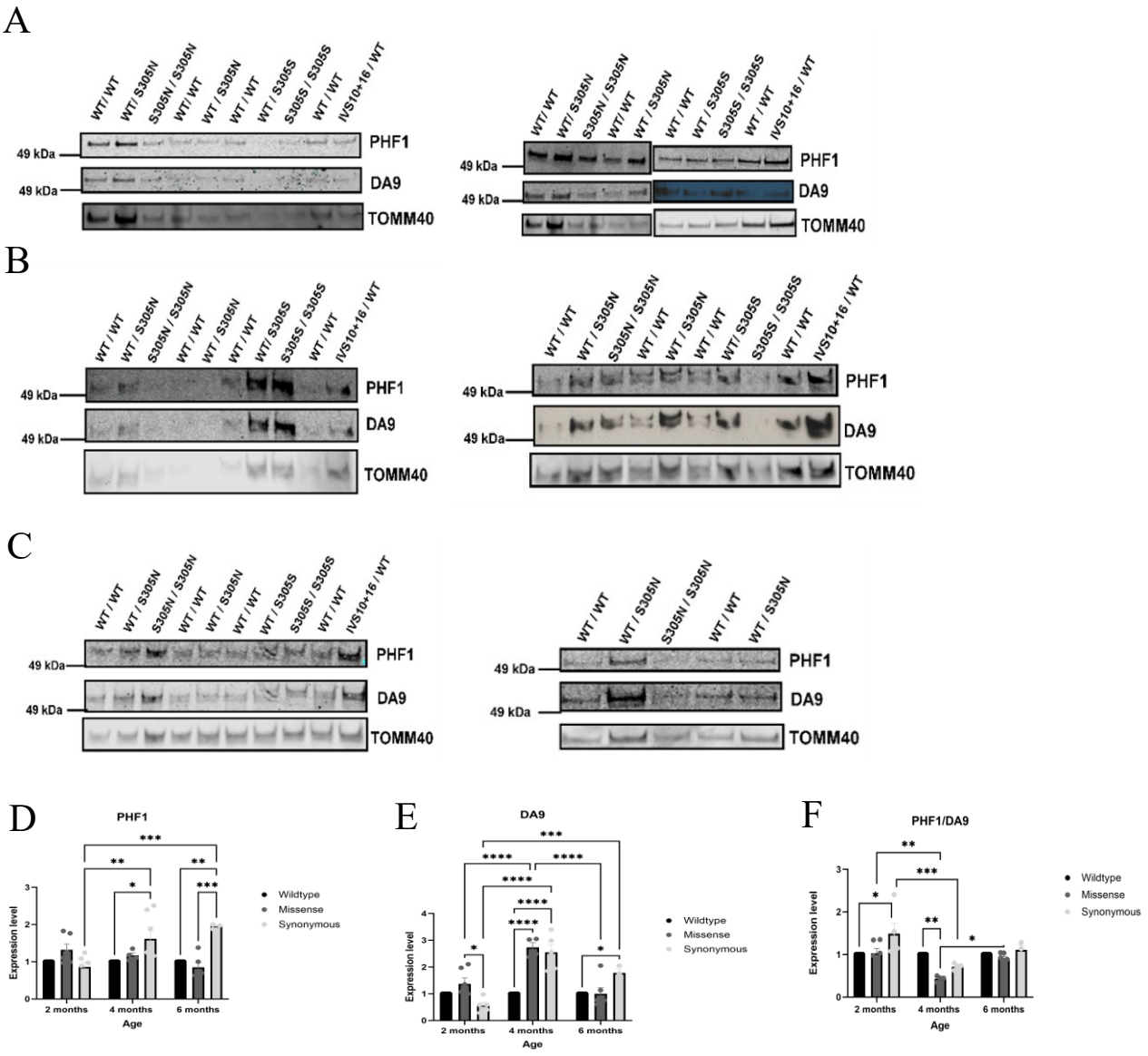

*Figure 9: Visualization of PHF1, DA9 and TOMM40 (housekeeping protein) of mitochondria isolates either by ECL or by fluorescence at A. two months (two replicates), B. four months (two replicates) and C. six months (two replicates of missense mutations and one replicate of synonymous mutation). Quantification of D. PHF1, E. DA9 and F. PHF1/DA9 in wild-type and mutation mitochondria isolates over time. Error bars indicate SEM. . Sample sizes used for analysis are D. n(2months) = 6, n(4months - missense) = 4, n(4months - synonymous) = 6, n(6months - missense) = 6, n(6months - synonymous) = 3, E. n(2months - missense) = 6, n(2months - synonymous) = 5, n(4months - missense) = 4, n(4months - synonymous) = 5, n(6months - missense) = 6, n(6months - synonymous) = 3 and F. n(2months - missense) = 6, n(2months - synonymous) = 5, n(4months - missense) = 4, n(4months - synonymous) = 5, n(6months - missense) = 6, n(6months - synonymous) = 3. Two-way ANOVA, Tukey's multiple comparisons test. *p < 0.05, **p < 0.01, ***p < 0,001, ****p < 0,0001.*

4.4 Significant increase of complex II was found in missense mutations at four months which was decreased again at six months

Lastly, a quantitative analysis of the five complexes with a role in OXPHOS was performed in mitochondria isolates over time, following a western blot (figure 10A, 10B, 10C). Due to technical constraints of the antibody, not all five complexes were visualized and quantified for each timepoint and each mutation.

The expression level of complex II (figure 10D) was significantly elevated for missense mutation at four months compared to synonymous mutation and decreased again at six months. For synonymous mutations, this expression level of complex II remained relatively equal to that in wild-type organoid lines over time. No significant differences were found in expression levels of complex V (figure 10E) between wild-type control lines and mutated lines over time. However, a slight decrease was found in synonymous mutation at four months and in missense mutation at six months.

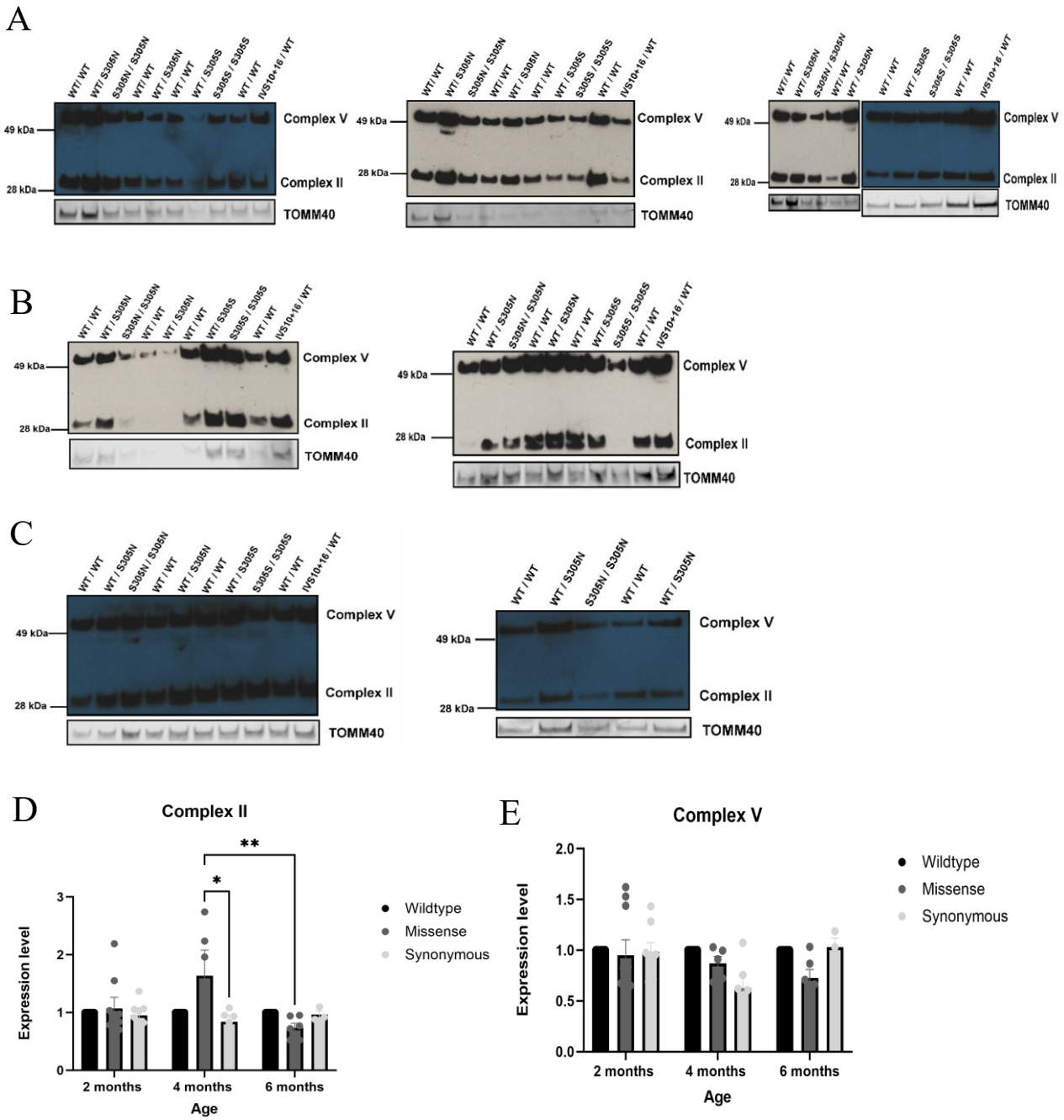

*Figure 10: Visualization of PHF1, DA9 and TOMM40 (housekeeping protein) of mitochondria isolates either by ECL or by fluorescence at A. two months (three replicates), B. four months (two replicates) and C. six months (two replicates for missense mutation and one replicate for synonymous mutation). Quantification of D. complex II and E. complex V in wild-type and mutation mitochondria isolates over time. Error bars indicate SEM. Sample sizes used for the analysis are D. n(2months) = 8, n(4months) = 5, n(6months - missense) = 6, n(6months - synonymous) = 3 and E. n(2months - missense) = 9, n(2months - synonymous) = 8, n(4months - missense) = 5, n(4months - synonymous) = 6, n(6months - missense) = 6 and n(6months - synonymous) = 3. Two-way ANOVA, Tukey's multiple comparisons test. *p < 0.05, **p < 0.01*

4.5 Mitochondrial mass was decreased between four and six months for both wild-type and missense mutations

PCR, followed by a quantification on the Agilent Technologies 4200 TapeStation, gave an indication on the number of mitochondria present per cell. A ladder was used to make sure PCR products were the same size as the expected product (figure 11).

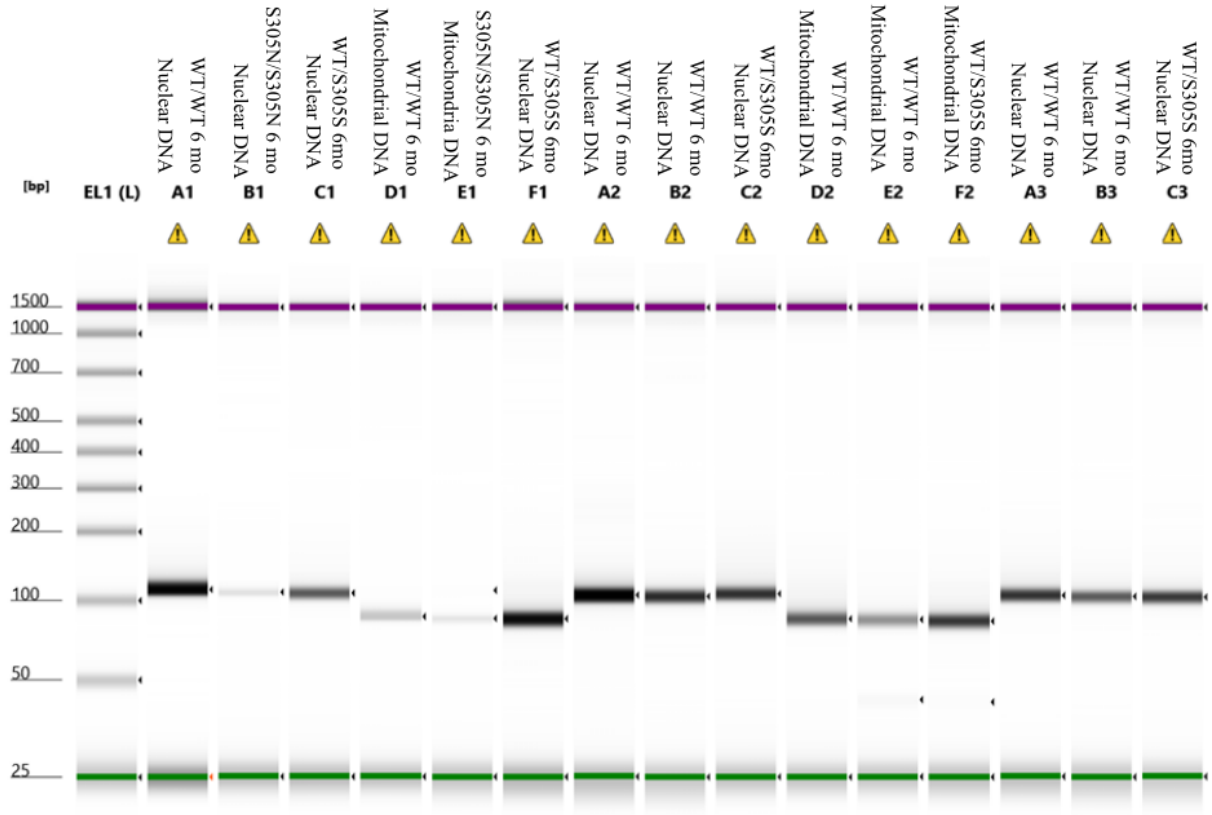

Figure 11: Representative image of the comparison of the PCR product in the sample to a ladder on the Agilent Technologies 4200 TapeStation. This allows us to make sure the PCR products are the same size as the expected product.

The mitochondrial copy number was compared between different mutant lines and their wild-type control line over time. This was done by determining the ratio between mitochondrial DNA and nuclear DNA (figure 12). No significant differences, according to ANOVA statistical analysis, were found comparing mutations with their wild-type within a certain time point. However, a decrease in mitochondrial copy number was found between four months and six months within wild-type and missense mutations. For synonymous mutations, a decrease was also present, but it was not significant according to ANOVA statistical analysis. These results are in contrast to the initial increase in mitochondrial mass for wild-type and both mutations.

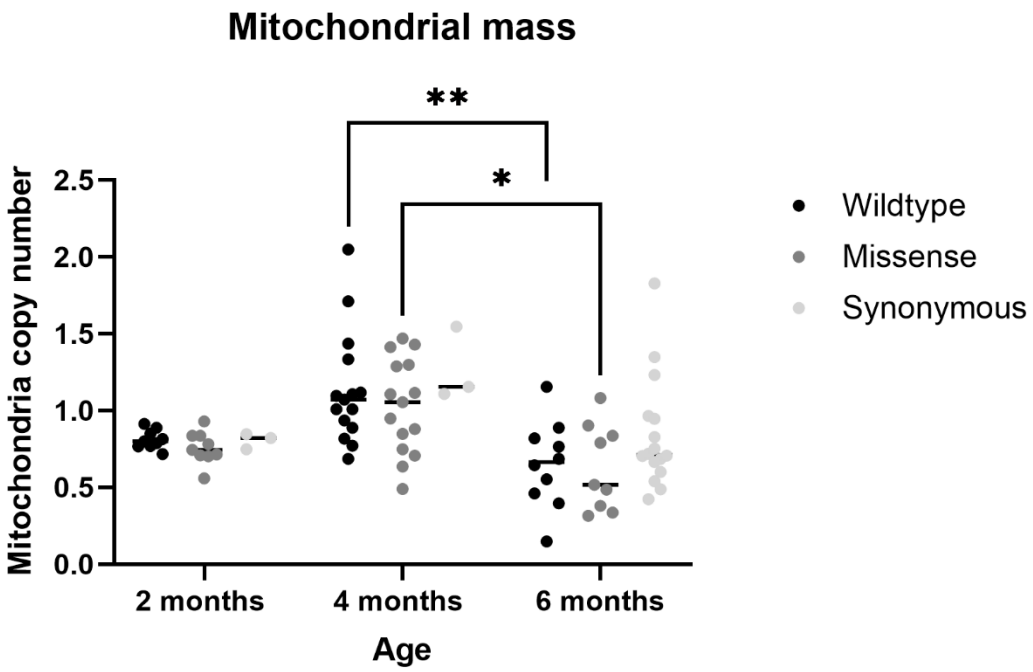

*Figure 12: Quantification of mitochondrial copy number of wild-type and mutation organoid lines over time following PCR. Error bars indicate SEM. Sample sizes used for the analysis are n(2months - missense) = 9, n(2months - synonymous) = 3, n(4months - missense) = 15, n(4months - synonymous) = 3 , n(6months - missense) = 9, n(6months - synonymous) = 16. Two-way ANOVA, Tukey multiple comparison test. *p < 0.05, **p < 0.01*

4.6 An increase in oxidative stress was only found in synonymous mutations, while significant changes in mitochondrial membrane potential were found in both mutations

Step-by-step gating strategy used in flow cytometry was (1) cells (figure 17A), (2) single cells (figure 17B), (3) Live/Dead Violet A subset (figure 17C), (4) MitoTracker, MitoSOX or TMRM. This allowed us to select cell population of interest based on (1) size and/or morphology, (2) single cells, (3) viable, live cells and (4) determine mitochondrial mass (figure 18A), oxidative stress (figure 18B) and membrane potential (figure 18C), respectively.

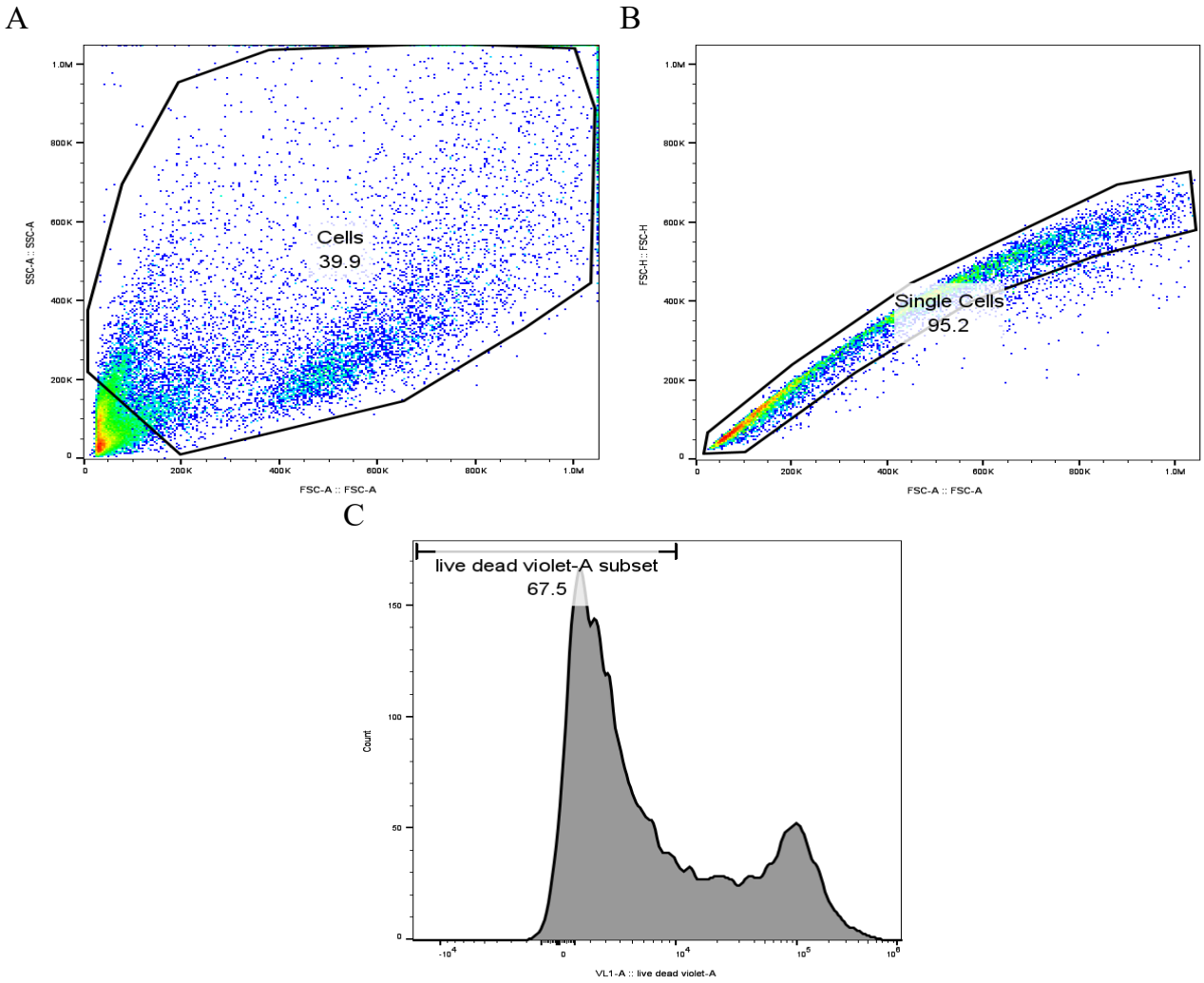

Figure 17: An example of the step-by-step gating strategy used in the flow cytometry following A. cells, B. single cells and C. Live/dead Violet A subset to identify live single cells for further quantification of MitoTracker, MitoSOX and TMRM. Abbreviations: SSC-A: side scatter - area, FSC-A : forward scatter - area, FSC-H: forward scatter – height, VL1-A: violet laser 1 – area

ANOVA statistical analysis indicated no significant difference in mitochondrial mass between wild-type organoid lines and both mutations over time (figure 18A). Even though not significant, mitochondrial mass was slightly increased in synonymous mutations at four months but decreased at six months.

To allow the quantification of oxidative stress per unit mitochondria, the ratio between oxidative stress and mitochondrial mass was calculated (figure 18B). Oxidative stress was significantly increased over time in synonymous mutations, resulting in a significant increase compared to the wild-type organoid lines and missense mutation organoid lines. The oxidative stress per unit mitochondria stayed relatively the same for missense mutation organoid lines over time and compared to wild-type control within time points.

Lastly, mitochondrial membrane potential was determined by measuring median fluorescent intensity of TMRM (figure 18C). In missense mutations, mitochondrial membrane potential progressively increased over time resulting in a significant difference between the mutation and its wild-type control at six months. In synonymous mutations, mitochondrial membrane potential increased at four months but later on decreased again, resulting in relatively equal membrane potential compared to the wild-type.

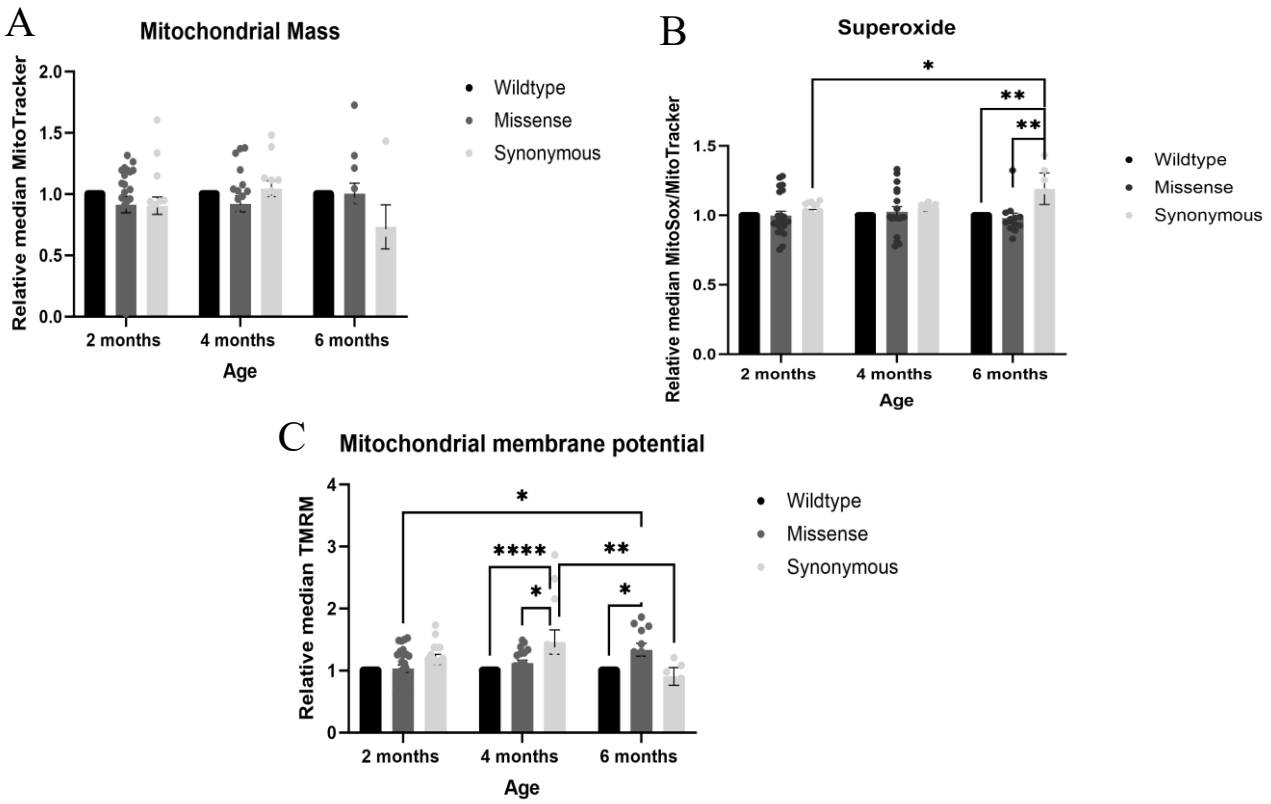

*Figure 18: Quantification of A. relative median MitoTracker, B. relative median MitoSOX/MitoTracker and C. relative median TMRM in wild-type, missense mutation and synonymous mutation organoid models by using flow cytometry. Quantification only includes single, live cells. Error bars indicate SEM. Sample sizes used for the analysis are A. n(2months - missense) = 24 , n(2months - synonymous) = 15, n(4months - missense) = 19, n(4months - synonymous) = 12 , n(6months - missense) = 12, n(6months - synonymous) = 5, B. n(2months - missense) = 23, n(2months - synonymous) = 15, n(4months - missense) = 19, n(4months - synonymous) = 12 , n(6months - missense) = 12, n(6months - synonymous) = 5 and C. n(2months - missense) = 27, n(2months - synonymous) = 15, n(4months - missense) = 19, n(4months - synonymous) = 12, n(6months - missense) = 12, n(6months - synonymous) = 5. Two-way ANOVA, Tukey multiple comparison test. *p < 0.05, **p < 0.01, ****p < 0,0001.*

4.7 A significant difference in acetylated tubulin between missense and synonymous mutation organoid lines was found at two months and four months

Organoid slices of wild-type, missense mutation and synonymous mutation were stained for total, acetylated and tyrosinated tubulin. Post-translational modifications, acetylation and tyrosination, indicate the stability of the tubulin in these organoids. For each time point, a representative image was added for wild-type (figure 13A, 14A, 15A), missense mutation (figure 13B, 14B, 15B) and synonymous mutation (figure 13C, 14C, 15C).

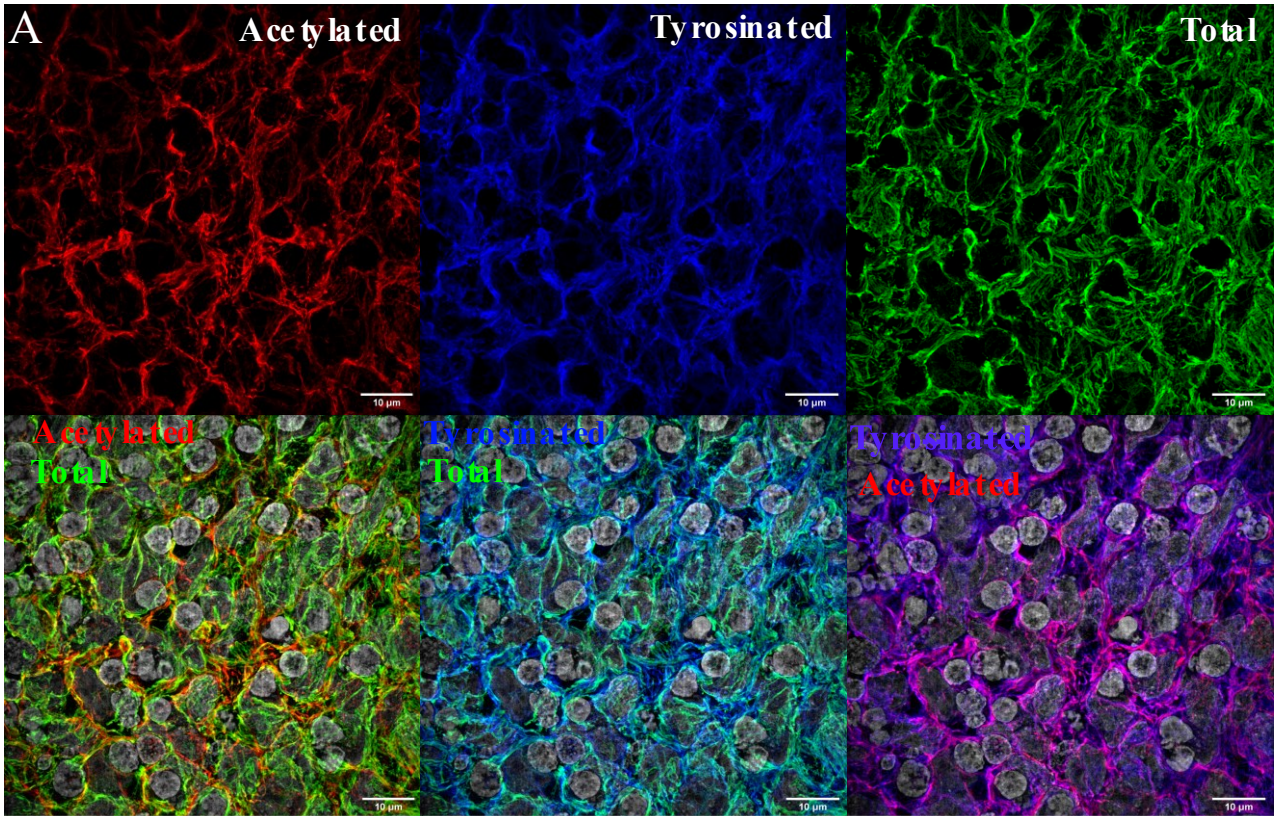

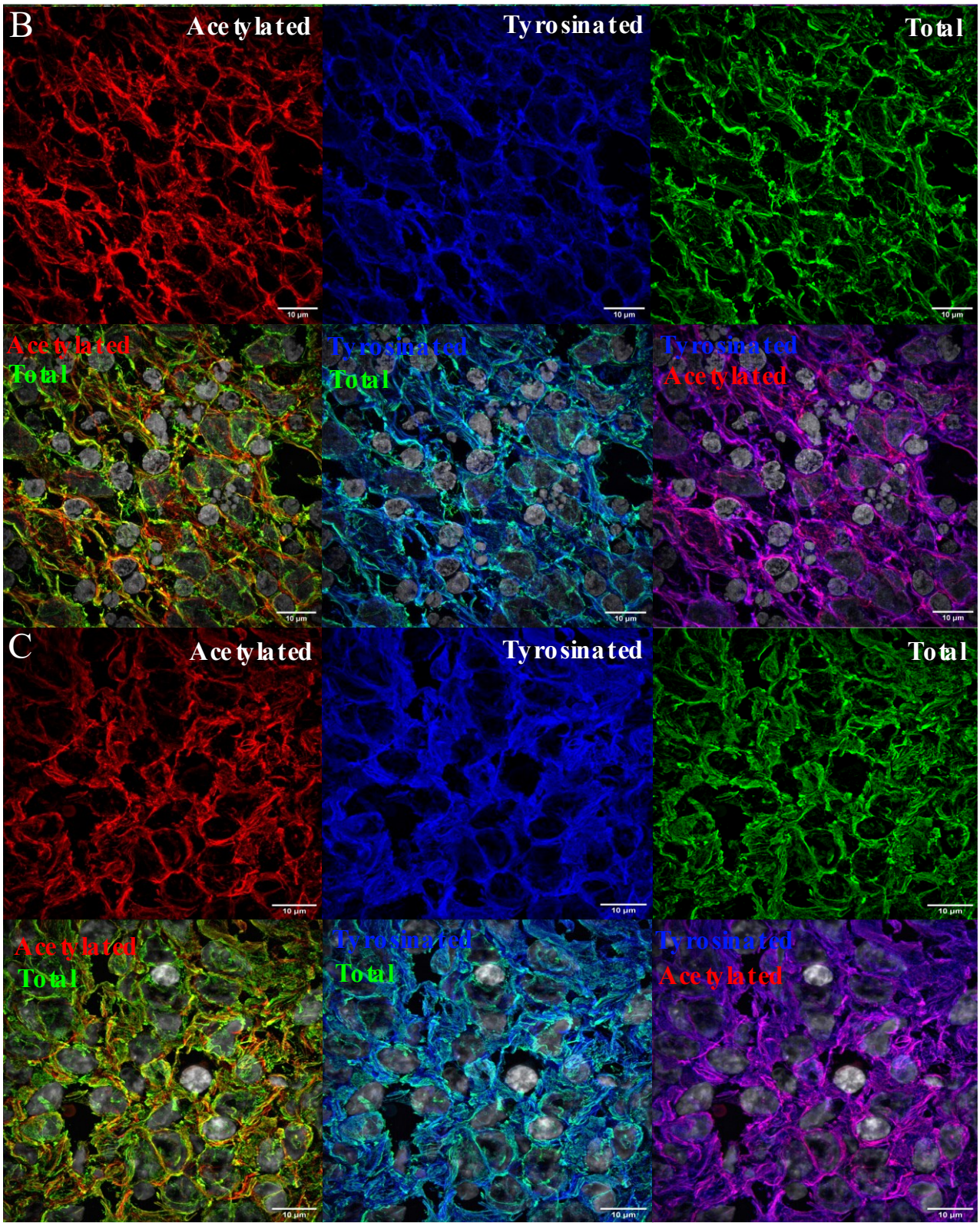

Figure 13: Representative images of A. wild-type, B. missense mutation and C. synonymous mutation organoid slices at two months. The amount of stable and dynamic tubulin was estimated by staining acetylated tubulin (red), tyrosinated tubulin (blue) and total tubulin (green) with a DAPI counterstaining (grey) showing nuclear morphology. Both acetylated and tyrosinated tubulin are normalized to total tubulin. The ratio between acetylated and tyrosinated tubulin has been calculated. Pictures were taken using Zeiss ELYRA 7 with Plan-Apochromat 63x/1.40 oil objective. Scale bars, 10 µm.

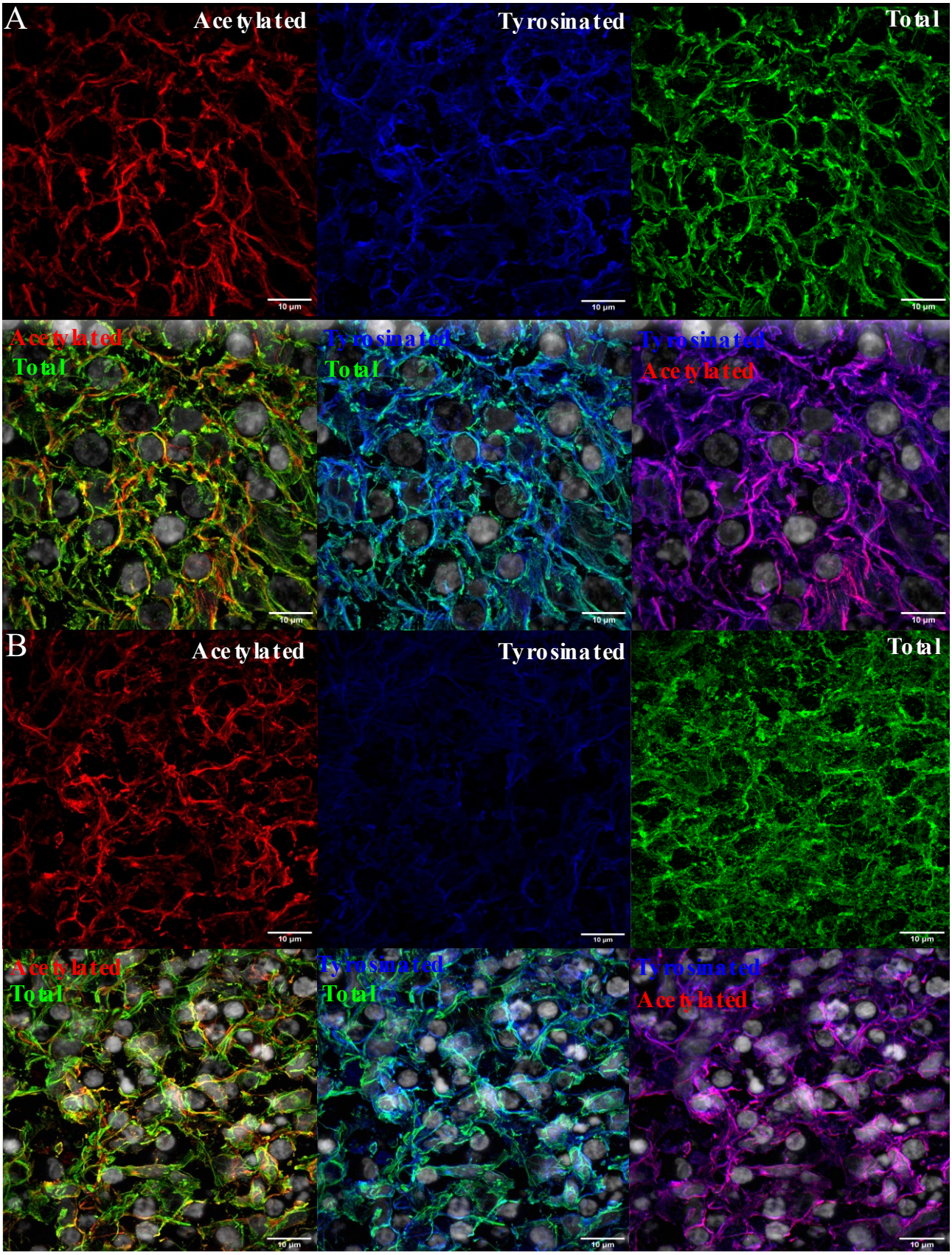
A
Acetylated
Tyrosinated
Total
Acetylated
Total
Tyrosinated
Total
Tyrosinated
Acetylated
B
Acetylated
Tyrosinated
Total
Acetylated
Total
Tyrosinated
Total
Tyrosinated
Acetylated
10 µm

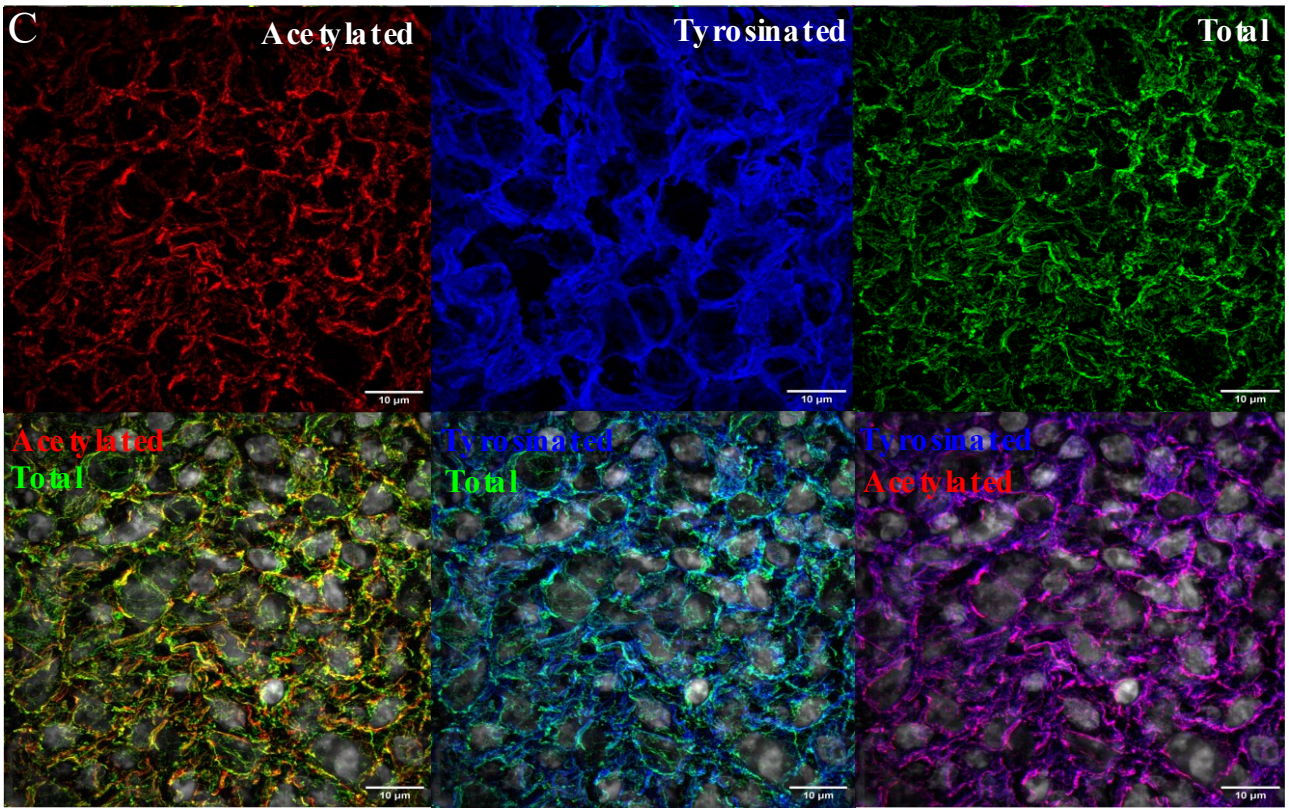

Figure 14: Representative images of A. wild-type, B. missense mutation and C. synonymous mutation organoid slices at four months. The amount of stable and dynamic tubulin was estimated by staining acetylated tubulin (red) and tyrosinated tubulin (blue) and total tubulin (green) with a DAPI counterstaining (grey) showing nuclear morphology. Both acetylated and tyrosinated tubulin are normalized to total tubulin. The ratio between acetylated and tyrosinated tubulin has been calculated. Pictures were taken using Zeiss ELYRA 7 with Plan-Apochromat 63x/1.40 oil objective. Scale bars, 10 µm.

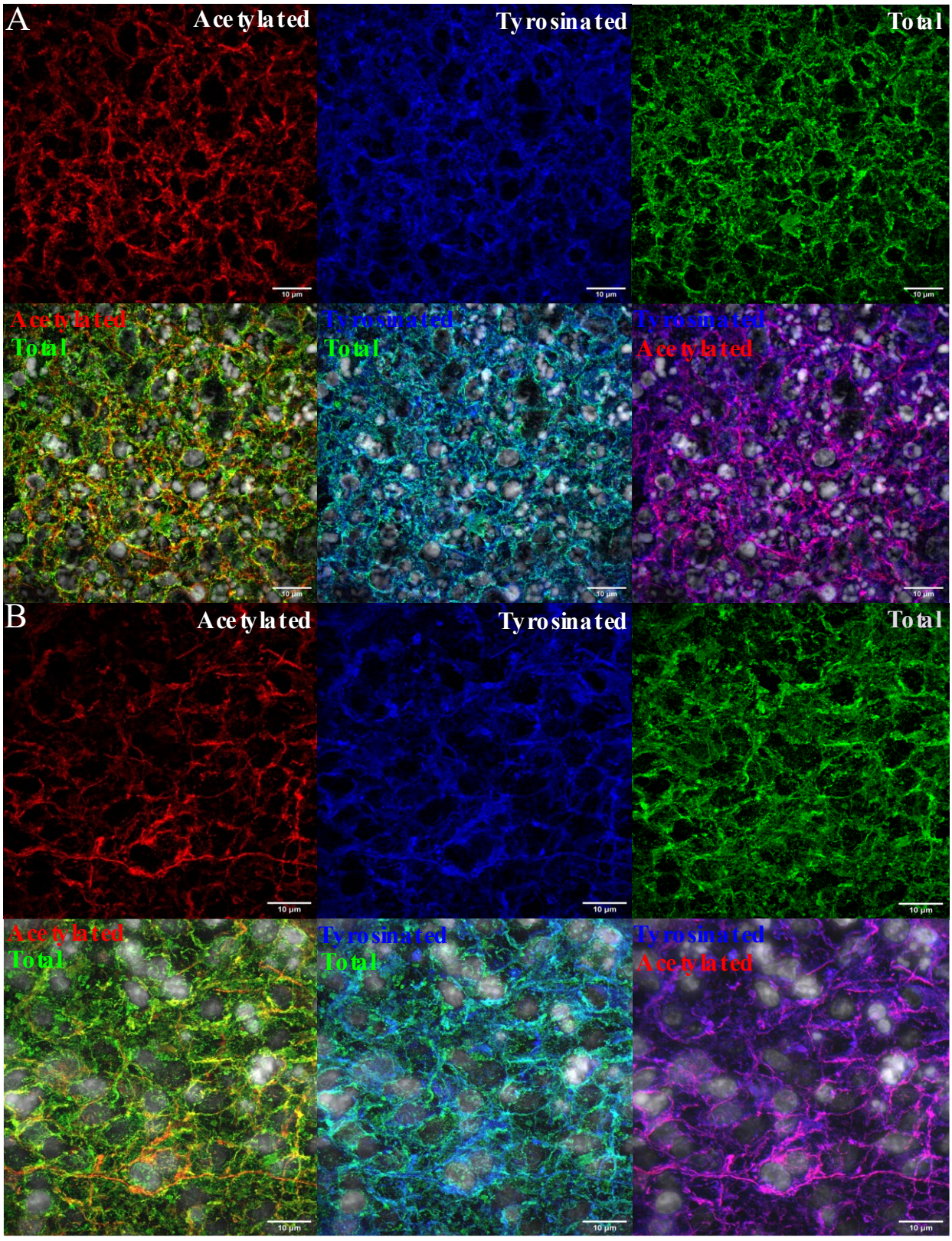

Figure 15: Representative images of A. wild-type and B. missense mutation organoid slices at six months. The amount of stable and dynamic tubulin was estimated by staining acetylated tubulin (red) and tyrosinated tubulin (blue) and total tubulin (green) with a DAPI counterstaining (grey) showing nuclear morphology. Both acetylated and tyrosinated tubulin are normalized to total tubulin. The ratio between acetylated and tyrosinated tubulin has been calculated. Pictures were taken using Zeiss ELYRA 7 with Plan-Apochromat 63x/1.40 oil objective. Scale bars, 10 µm.

Acetylated tubulin (figure 16A), tyrosinated tubulin (figure 16B) and the ratio between both (figure 16C) were quantified and compared between wild-type and mutation organoid lines over time. The amount of tyrosinated tubulin decreased slightly in both mutations in comparison to their wild-type organoid lines at four months. However, a significant difference was only found in acetylated tubulin between the missense mutation and the synonymous mutation at two months and four months. The organoids with a missense mutation had elevated levels of acetylated tubulin compared to their wild-type at two months. In contrast, organoids with a synonymous mutation had slightly decreased levels of acetylated tubulin in comparison to their wild-type at two and four months.

Despite the significant difference in acetylated tubulin between the two mutations, there was no significant difference between missense and synonymous mutation when calculating the ratio between acetylated and tyrosinated tubulin, reflecting the balance between stable and unstable microtubules. However, even though not significant, the ratio between acetylated and tyrosinated tubulin was increased for the missense mutation, which was lost gradually over time. The ratio was slightly decreased for synonymous mutations at two months and remained decreased at four months.

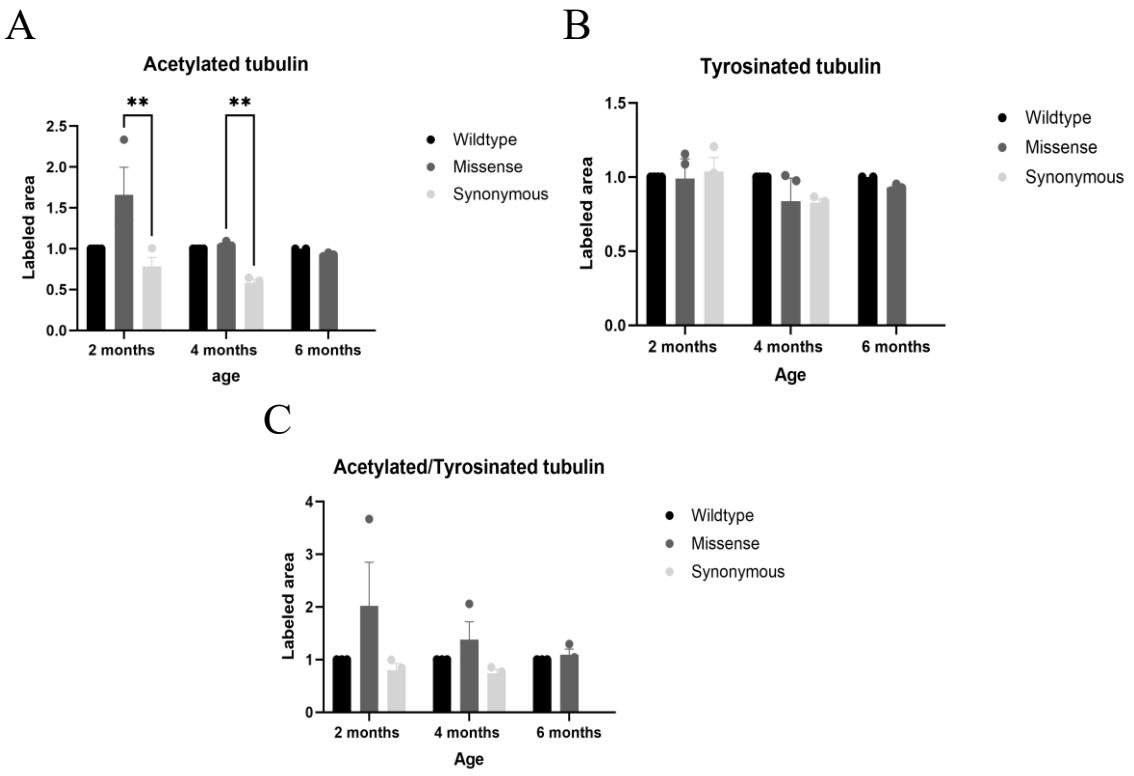

*Figure 16: Quantification of A. acetylated tubulin, indicating stable tubulin, B. tyrosinated tubulin, indicating dynamic tubulin, and C. the ratio of acetylated tubulin and tyrosinated tubulin in wild-type, missense mutation and synonymous mutation organoid slices over time. Quantification was performed by calculating labeled areas for each fluorophore in imageJ and acetylated and tyrosinated tubulin was normalized to total tubulin. Error bars indicate SEM. Sample size used for the analysis is n = 3. Two-way ANOVA, Tukey multiple comparison test. **p < 0.01*

5. Discussion

5.1 An increased turnover of 4R tau could lead to decreased total tau levels in synonymous mutations at early stages

Given the percentage of FTD patients with inclusions showing tau aggregation, it is important to understand the exact role of tau and their tangles in the development of FTD. Are tau proteins and the formation of tau tangles the trigger for the development of FTD or are they the result of earlier abnormalities in these patients? One hypothesis, researched for years, is that the hyperphosphorylation limits the affinity of tau proteins to bind microtubules eventually leading to formation of tangles (Goedert et al., 1992; Martin et al., 2011; Meraz-Ríos et al., 2010). However, results showed only a significant difference in total tau between two-months-old and four-months-old synonymous mutation organoid lines, but there were no differences in phosphorylation of tau on the PHF1 epitope.

DA9 is an antibody used for staining total tau and so does not differentiate between 3R and 4R tau proteins and tau tangles and physiological tau. The decreased levels of total tau at four months could actually indicate the degradation of tau, which would be contrary to the belief of tau tangles being involved in the development of FTD. However, the synonymous mutations have been shown to increase wild-type 4R tau levels at early developmental stages in the organoid models (Bowles et al., 2024) and the turnover rate of 4R tau is faster than 3R tau (Sato et al., 2018). The combination of increased levels of 4R tau and its increased turnover rate in comparison to 3R tau could explain the decrease of total tau levels in synonymous mutations (Bowles et al., 2024; Sato et al., 2018). It is still unclear why exactly 4R tau has a faster turnover. However, an explanation could be found in the degradation mechanisms of tau involving hsp70/hsp90/CHIP chaperone system. Heat shock protein 70 (Hsp70) can recognize abnormal tau and recruit carboxy-terminus of hsc70-interacting protein (CHIP) via its tetratricopeptide repeat domain. CHIP induces ubiquitination on the microtubule-binding domains, more specifically the aggregation motif present in R2 and R3 in the *MAPT* gene. So even though the extra repeat domain has an extra aggregation motif present, it is also a binding site for hsp70 chaperones, which inhibits aggregation as long as soluble tau is present (Mok et al., 2018; Petrucelli, 2004). If tau is degraded early on, it cannot bind to microtubules or mitochondria, potentially leading to the development of FTD.

At six months, the expression levels of total tau in synonymous mutations rise again to a level similar to the wild-type lines. This could suggest that aggregation has started, halting the increased turnover of 4R tau seen in earlier stages. Missense mutations increase mutated 4R tau, which might slow down the normally increased turnover, explaining why this significant decrease in total tau is not seen in missense mutation organoid lysates at four months.

5.2 Hyperstabilized microtubules due to missense mutations could potentially impact mitochondrial transport

Stabilization of tubulin, a key component of microtubules, is one of the main functions of tau. By introducing mutated and wild-type 4R tau, the missense mutation and synonymous mutation might also impact tubulin stability. Tubulin stability could be indicated by possible post-translational modifications of tubulin, namely acetylation and tyrosination.

Results showed a significant difference in acetylated tubulin between missense and synonymous *MAPT* gene mutations, with respectively increased and decreased levels of acetylated tubulin. An increase in acetylated tubulin, seen in missense mutations, could indicate a shift towards the long-lived microtubules while a decrease in acetylated tubulin, seen in synonymous mutations, could indicate a decrease in long-lived microtubule population. This difference in amount of acetylated tubulin between the two mutations could potentially be a genotype-specific difference involved in the development of FTD. There was no significant change in tyrosinated tubulin, so this indicates that there might be a change in abundance of long-lived microtubule population but not necessarily in the number of dynamic microtubules.

However, mainly the balance between stable and unstable microtubules is important for the maintenance of the cytoskeleton and the health of neurons in early stages of development. Not only could too many dynamic microtubules potentially cause neurodegenerative diseases, but also too many stable microtubules could induce certain abnormalities potentially leading to pathology (Dubey et al., 2015). The ratio between acetylated and tyrosinated tubulin was increased in organoids with a missense mutation at two months, indicating hyperstabilized tubulin in early stages.

A mouse model of neurodegenerative diseases has shown that the stability of tubulin could exist in two stages, starting with a stage characterized by hyperstable microtubules and ending with a stage of unstable microtubules (Fanara et al., 2010). An early stage of hyperstable microtubules was also seen in the missense mutation organoid lines, followed by restored balance between stable and unstable microtubules at six months. These results are counterintuitive with what is expected in missense mutations. Missense mutations will increase the level of mutated 4R tau, which is thought to have less affinity for microtubules. However, this early hyperstabilized phase could be explained by compensatory mechanisms. Previously, it has been shown that a mutation of tau proteins, affecting its ability to stabilize microtubules, will increase expression of compensatory proteins like microtubule-associated protein 1A (MAP1A) leading to hyperstabilization (Harada et al., 1994). However, as toxic tau accumulates over time, the proteins could cause the sequestering of MAP1A and other microtubule-associated proteins (Iqbal et al., 2005), resulting in the second phase characterized by unstable microtubules. This second phase is not seen in our results but is possibly only apparent later in the development. This imbalance in stable/unstable microtubules is most prominent at two months. The rapid switch in the number of stable tubulin might explain the rapid progression and early onset in patients with a missense mutation (Bowles et al., 2024).

However, in synonymous mutations, acetylated tubulin is slightly decreased at two months and four months, but it is less prominent than the increase seen in missense mutations. This could be due to the high turnover of 4R tau, resulting in less tau available, confirmed by western blot results, to bind to and stabilize tubulin (Sato et al., 2018). The turnover rate of 4R tau might outweigh compensatory mechanisms, leading to a net decrease in stable, long-lived microtubules. Also, a small decrease in tyrosinated tubulin was found in synonymous mutations. The decrease in both acetylated and tyrosinated tubulin and limited difference in ratio between the two could indicate a switch in post-translational modifications or tubulin isotype while maintaining the crucial balance between stable and unstable tubulin. In a previous study, a switch to detyrosinated tubulin and Δ2-tubulin was found, leading to synapse loss related to Alzheimer's disease (Peris et al., 2022).

5.3 Altered microtubules dynamics could impact mitochondria

The cytoskeleton, consisting of tubulin, has many functions contributing to cell health. One of those is the transport of organelles, including mitochondria. This could lead to an accumulation of mitochondria, possibly dysfunctional, in the soma. Changes in the mitochondrial mass could be an indirect effect of destabilization of microtubules in tauopathies.

The rapid increase in stable microtubules in early stages of the development of the disease, seen in missense mutations, could impact mitochondrial transport. Dynein and kinesin are motor proteins involved in the transport of organelles (Dixit et al., 2008). These bind to microtubules in competition with microtubule-associated proteins (Dixit et al., 2008; Ebneth et al., 1998). The increase in microtubule-associated proteins as a compensatory mechanism for mutated 4R tau could outcompete dynein and kinesin, blocking transport of organelles (Ebneth et al., 1998). The hyperstabilization of microtubules in missense mutation organoid lines could corroborate earlier results from the lab using live imaging indicating slower transport of mitochondria. These results could lead to the hypothesis of genotype-specific involvement of microtubules and mitochondrial transport in the development of FTD.

PCR and quantification of mitochondrial copy number showed no significant difference between wild-type and mutation lines within time points. This was confirmed by OXPHOS staining in western blot and flow cytometry (MitoTracker). This could indicate that there is no difference in mitochondrial mass induced by neither missense mutation nor synonymous mutation. However, these tests do not discriminate between mitochondria in different locations. The total mitochondrial mass might not be impacted but the mitochondrial mass at synaptic level might be due to loss of mitochondrial transport, which is not tested by western blot, flow cytometry or PCR followed by quantification.

5.4 Two-way interaction between mitochondria and tau might play a role in patients with a synonymous mutation

The impact of tau on mitochondria might be more direct in FTD patients with a missense or synonymous *MAPT* mutation. The interaction between tau protein and mitochondria is bidirectional, both impacting each other.

To determine if hyperphosphorylation of tau proteins was present, specifically those interacting with mitochondria, a western blot with PHF1 staining was performed using mitochondrial isolates. Phosphorylation at S396-S404 has been indicated in possibly inducing a conformational change which could promote the formation of tau tangles (Cantrelle et al., 2021). Significant changes in relative phosphorylation of tau, normalized to total tau, implied a potential genotype-specific role of phosphorylated tau through its interaction with mitochondria. Synonymous mutations showed an increase in relative PHF1 levels at two months, indicating hyperphosphorylation of tau. Phosphorylation was decreased at four months and again slightly increased at six months. This fluctuation in relative PHF1 levels could be due to the sudden surge in total tau at four months, which is seen in both synonymous and missense mutations. The early hyperphosphorylation seen at two months could imply that phosphorylation of tau, interacting with mitochondria, might be one of the triggers, leading to disruption or alterations of other mechanisms. Since this significant difference in phosphorylation of tau was only seen in mitochondrial isolates, this could indicate that the mutation of the *MAPT* gene mainly impacts phosphorylation of tau, interacting with mitochondria, which might be overshadowed in organoid lysates.

Previous research has shown a relationship between hyperphosphorylation and mitochondrial dysfunction in synaptic mitochondria, which are fundamental in synaptic transmission and memory formation (Picard, 2015; Torres et al., 2021). In the research of Torres et al. (2021), hyperphosphorylation at PHF1 epitope was tested in the hippocampus. It was shown that the pathological tau mainly accumulates in synaptic mitochondria, which increases during ageing. Ageing is still a major risk factor in neurodegenerative diseases, like FTD. It was shown that pathological phosphorylation and aggregation of tau could cause synaptic impairment (Torres et al., 2021). Tests performed in this thesis do not differentiate between mitochondria depending on their location. However, our results combined with these findings could indicate a potential role of hyperphosphorylated tau at the synapse in the early stages of disease development in patients with a synonymous mutation and accumulation of tau at mitochondria in both mutations.

It was not only shown that pathological accumulation of tau could induce mitochondrial dysfunction, but mitochondrial dysfunction can also induce the accumulation of tau. The interaction between accumulation of tau and mitochondrial dysfunction is a two-way street both affecting and inducing each other. Specifically, a study in human fibroblasts has shown that oxidative stress, due to mitochondrial dysfunction, can induce the accumulation of tau, potentially through activating p38 MAPK (Saitoh et al., 1998). This study showed increase in total tau and increase and mislocalization of phosphorylated tau (AT8). Also increased nuclear PHF1 staining was found with increased oxidative stress (Ibáñez-Salazar et al., 2017). An increase in oxidative stress was found in synonymous mutation organoid lines at six months, with a small increase in hyperphosphorylated tau in comparison to levels of hyperphosphorylated tau in four months. This could indicate the role of oxidative stress in the hyperphosphorylation of tau and a potential two-way adverse relationship between tau and mitochondria. Also, total tau, interacting with mitochondria, was increased in synonymous mutations at four months and six months, which corresponds to the findings in the study of Ibáñez-Salazar et al. (2017). The accumulation of total tau could disrupt the mitochondrial distribution within a cell (Kopeikina et al., 2011) and could also increase glycogen synthase kinase-3β (GSK3β) activity, which could induce hyperphosphorylation of tau proteins (Alquezar et al., 2021), which is reflected in results at six months.

5.5 Mutations in MAPT gene might impact functionality of mitochondria instead of mitochondrial mass

An increase in mutated and wild-type 4R tau might impact the functionality of mitochondria. In synonymous mutations, there was an increased mitochondrial membrane potential at four months. This increase was no longer present at six months. A study from Esteras et al. (2017) in IVS10+16 iPSC models, has also shown hyperpolarization of mitochondria despite reduced mitochondrial respiration. This is consistent with the results of Bowles et al. (2024) showing reduced mitochondrial respiration, performing a Seahorse mitochondrial stress test, in combination with increased mitochondrial membrane potential, performing flow cytometry with TMRM staining. An accumulation of human full-length tau (4R) has shown to potentially lead to deficits in PTEN-induced kinase 1 (PINK1) and Parkin complexes and mitophagy, resulting in an increase of mitochondrial membrane potential (Hu et al., 2016). This corresponds to our results in synonymous mutations, which induced an increase in total tau (DA9) in mitochondria isolates, possibly resulting in increased mitochondrial membrane potential (TMRM).

Mitochondrial membrane potential was also increased in missense mutations at six months, when levels of total tau (DA9) in mitochondria isolates were similar to levels in wild-type. However, the hyperpolarization of the mitochondrial membrane potential was accompanied by an increase in complex II in missense mutations at four months. Upregulation of complex II, if combined with dysfunction in complex I, might be involved in the increase in mitochondrial membrane potential (Abramov et al., 2010).

An increase in mitochondrial membrane potential could result in cell death and neurodegeneration. This is due to the role it plays in oxidative stress. Hyperpolarized mitochondria, which were found in IVS10+16 FTD neurons, caused an increase in ROS (Esteras et al., 2017). Flow cytometry results showed an increase in mitochondrial membrane potential at four months and an increase in oxidative stress at six months in synonymous mutations, implying a temporal relationship between both. The increase in oxidative stress was not present in missense mutation organoid lines, despite the increase in mitochondrial membrane potential at six months. These results might indicate that hyperpolarization of the mitochondrial membrane drives the generation of oxidative stress. The eventual increase in oxidative stress could lead to apoptosis or calcium-induced cell death (Circu & Aw, 2010; Esteras et al., 2022).

5.6 Possible caveats and future possibilities

FTD is a progressive disease, which means that processes involved in the development of FTD have been impacted long before symptoms appear and treatment will start. Organoids are good models for studying genetic drivers and early mechanisms leading to the development of the disease. However, ageing plays an important role in neurodegenerative diseases, but is not easy to model in organoids, which in this thesis are only two months, four months and six months old. It is possible that, when using these models, important ageing mechanisms involved in the development of FTD are not detected. Organoids are also limited in their capability to form functional circuits and still contain embryonic markers when matured (Andrews & Kriegstein, 2022). However, these models are still a good addition to post-mortem and clinical studies, specifically for studying the early stages of the development of FTD and what might be a trigger for the formation of tau tangles. This could lead to the identification of early-stage biomarkers, which is important for early treatment and prevention of the disease (Urrestizala-Arenaza et al., 2024).

Most tests used in this thesis were performed on whole tissues, which contains multiple different cell types. However, mutations in *MAPT* gene and their involvement in FTD development have been hypothesized to impact neurons. By not isolating neurons, other cell types which are not impacted by *MAPT* mutations might mask the changes that occur in neurons. This could lead to false conclusions made based on the results. Isolation of neurons can be performed on forebrain organoids using enzymatic digestion and cell sorting by marking neurons with antibodies (Sloan et al., 2017). However, enzymatic digestion and cell sorting are invasive techniques that could impact key structures being studied like mitochondria and microtubules. This would interfere with the results and could also lead to false conclusions.

Many tests are performed in scope of the involvement of mitochondria in the development in FTD. Most tests performed in this thesis are related to the number of mitochondria present. A significant difference in the level of mitochondria could indicate their involvement in development of FTD. However, these tests do not discriminate mitochondria based on their location or functionality. Microtubules transport mitochondria, which has been discussed in scope of the results as well. It might be interesting to include localization of mitochondria and their interaction with tau in combination with the data on microtubules stability to understand the potential genotype-specific impact on the transport of mitochondria better. Live imaging, following mitochondrial transport, has been performed prior to my internship in the lab. A proximity ligation assay between tau and mitochondria and tau and tubulin is planned in the lab after my internship. These tests could give more insight into the genotype-specific impact of tau on microtubules and subsequently mitochondrial transport and the interaction of tau with mitochondria directly. Studying localization of mitochondria could give insight into the potential impact of location on the interaction between tau and mitochondria. This could be performed by staining organoids for PHF1 (phosphorylated), TOMM40 (mitochondria) and synaptophysin (pre-synaptic), combined with imaging on Zeiss Elyra 7.

In the flow cytometry, staining for MitoSOX and TMRM was performed which tests for oxidative stress and mitochondrial membrane potential, respectively. These could indicate functionality of mitochondria but are not direct measurements of the ability of mitochondria to produce ATP via OXPHOS. Additionally, more direct tests might give us a better understanding if the functionality itself might be affected in patients with FTD and if there might be genotype-specific differences. Also, testing the functionality of individual complexes involved in OXPHOS might give interesting insights on how mutations in *MAPT* gene exactly impact mitochondria and OXPHOS.

One potential assay, testing for the efficiency of the ATP production via OXPHOS, is an extracellular flux assay. This is an assay that measures the oxygen levels. Oxygen levels are a direct indicator of OXPHOS due to the fact that oxygen is the last electron acceptor in the electron transport chain and so oxygen is consumed as long as the electron transport chain is active. Besides the assay measuring changes in oxygen levels, it also measures changes in proton levels. The test can be performed on organoids or isolated mitochondria (Ludikhuize et al., 2021; Yoo et al., 2024). Another option is quantifying the ATP levels. Even though this is less specific, since ATP could come from other sources like glycolysis, it would be a good indication of the effectiveness of OXPHOS by the mitochondria. You can do this by using a luciferase-based assay, for example CellTiter-Glo luminescent assay. This assay uses a luciferase/luciferin reaction, in which the luminescence is proportional to the level of ATP (Duong et al., 2021).

6. Conclusion

FTD is a very heterogenous disease in every aspect, including genetics, neuropathology and clinical features. This heterogeneity makes studying and treating FTD very complicated. With this thesis, we focused on FTD-tau, specifically on patients with missense and synonymous mutations in the *MAPT* gene leading to FTD. The aim of this study was to deepen the understanding of the impact of missense and synonymous *MAPT* mutations on tau, microtubules and mitochondria.

By comparing wild-type, missense mutated and synonymous mutated organoid cell lines, we discovered potential genotype-specific mechanisms, both leading to FTD. Results of tubulin stability combined with previously obtained results on mitochondrial transport imply that missense mutations in *MAPT* gene might impact microtubule stability. In contrast, mitochondrial transport appears less impacted in synonymous mutations, but functionality of the mitochondria was likely impacted, which could involve the interplay between oxidative stress and hyperphosphorylation of tau protein, directly interacting with mitochondria. The comparison over time, at two months, four months and six months, revealed a potential cascade of pathological mechanisms eventually leading to FTD.

Understanding genotype-specific mechanisms could lead to more personalized treatment opportunities. By performing the study in wild-type, missense and synonymous organoid lines over time, we were able to further our understanding of the disease mechanisms involved in early stages, which could potentially lead to early detection and treatment, resulting in potential cure and prevention of the disease entirely.

7. References

Abramov, A. Y., Smulders-Srinivasan, T. K., Kirby, D. M., Acin-Perez, R., Enriquez, J. A., Lightowlers, R. N., Duchen, M. R., & Turnbull, D. M. (2010). Mechanism of neurodegeneration of neurons with mitochondrial DNA mutations. *Brain*, *133*(3), 797–807. https://doi.org/10.1093/brain/awq015

Ahmad, F., Pienkowski, T., & Baas, P. (1993). Regional differences in microtubule dynamics in the axon. *The Journal of Neuroscience*, *13*(2), 856–866. https://doi.org/10.1523/JNEUROSCI.13-02-00856.1993

Alavi Naini, S. M., & Soussi-Yanicostas, N. (2015). Tau Hyperphosphorylation and Oxidative Stress, a Critical Vicious Circle in Neurodegenerative Tauopathies? *Oxidative Medicine and Cellular Longevity*, *2015*, 1–17. https://doi.org/10.1155/2015/151979

Alquezar, C., Arya, S., & Kao, A. W. (2021). Tau Post-translational Modifications: Dynamic Transformers of Tau Function, Degradation, and Aggregation. *Frontiers in Neurology*, *11*. https://doi.org/10.3389/fneur.2020.595532

Andrews, M. G., & Kriegstein, A. R. (2022). Challenges of Organoid Research. *Annual Review of Neuroscience*, *45*(1), 23–39. https://doi.org/10.1146/annurev-neuro-111020-090812

Arai, T., Hasegawa, M., Akiyama, H., Ikeda, K., Nonaka, T., Mori, H., Mann, D., Tsuchiya, K., Yoshida, M., Hashizume, Y., & Oda, T. (2006). TDP-43 is a component of ubiquitin-positive tau-negative inclusions in frontotemporal lobar degeneration and amyotrophic lateral sclerosis. *Biochemical and Biophysical Research Communications*, *351*(3), 602–611. https://doi.org/10.1016/j.bbrc.2006.10.093

Baborie, A., Griffiths, T. D., Jaros, E., McKeith, I. G., Burn, D. J., Richardson, A., Ferrari, R., Moreno, J., Momeni, P., Duplessis, D., Pal, P., Rollinson, S., Pickering-Brown, S., Thompson, J. C., Neary, D., Snowden, J. S., Perry, R., & Mann, D. M. A. (2011). Pathological correlates of frontotemporal lobar degeneration in the elderly. *Acta Neuropathologica*, *121*(3), 365–371. https://doi.org/10.1007/s00401-010-0765-z

Bang, J., Spina, S., & Miller, B. L. (2015). Frontotemporal dementia. *The Lancet*, *386*(10004), 1672–1682. https://doi.org/10.1016/S0140-6736(15)00461-4

Bardai, F. H., Ordonez, D. G., Bailey, R. M., Hamm, M., Lewis, J., & Feany, M. B. (2018). Lrrk promotes tau neurotoxicity through dysregulation of actin and mitochondrial dynamics. *PLOS Biology*, *16*(12), e2006265. https://doi.org/10.1371/journal.pbio.2006265

Binder, J. R. (2015). The Wernicke area. *Neurology*, *85*(24), 2170–2175. https://doi.org/10.1212/WNL.0000000000002219

Bowles, K. R., Pedicone, C., Pugh, D. A., Oja, L.-M., Sousa, F. H., Keavey, L. K., Fulton-Howard, B., Weitzman, S. A., Liu, Y., Chen, J. L., Disney, M. D., & Goate, A. M. (2024). Development of MAPT S305 mutation human iPSC lines exhibiting elevated 4R tau expression and functional alterations in neurons and astrocytes. *Cell Reports*, *43*(12), 115013. https://doi.org/10.1016/j.celrep.2024.115013

Boxer, A. L., Gold, M., Huey, E., Gao, F., Burton, E. A., Chow, T., Kao, A., Leavitt, B. R., Lamb, B., Grether, M., Knopman, D., Cairns, N. J., Mackenzie, I. R., Mitic, L., Roberson, E. D., Van Kammen, D., Cantillon, M., Zahs, K., Salloway, S., … Cummings, J. (2013). Frontotemporal degeneration, the next therapeutic frontier: Molecules and animal models for frontotemporal degeneration drug development. *Alzheimer's & Dementia*, *9*(2), 176–188. https://doi.org/10.1016/j.jalz.2012.03.002

Buchholz, S., & Zempel, H. (2024). The six brain-specific TAU isoforms and their role in Alzheimer's disease and related neurodegenerative dementia syndromes. *Alzheimer's & Dementia*, *20*(5), 3606–3628. https://doi.org/10.1002/alz.13784

Buchsbaum, M. S. (2004). Frontal Cortex Function. *American Journal of Psychiatry*, *161*(12), 2178–2178. https://doi.org/10.1176/appi.ajp.161.12.2178

Buratti, E., & Baralle, F. E. (2010). The multiple roles of TDP-43 in pre-mRNA processing and gene expression regulation. *RNA Biology*, *7*(4), 420–429. https://doi.org/10.4161/rna.7.4.12205

Carl Wernicke. (1874). *Der aphasische symptomencomplex*.

Chan, D. C. (2006). Mitochondria: Dynamic Organelles in Disease, Aging, and Development. *Cell*, *125*(7), 1241–1252. https://doi.org/10.1016/j.cell.2006.06.010

Chen, J. L., Moss, W. N., Spencer, A., Zhang, P., Childs-Disney, J. L., & Disney, M. D. (2019). The RNA encoding the microtubule-associated protein tau has extensive structure that affects its biology. *PLOS ONE*, *14*(7), e0219210. https://doi.org/10.1371/journal.pone.0219210

Circu, M. L., & Aw, T. Y. (2010). Reactive oxygen species, cellular redox systems, and apoptosis. *Free Radical Biology and Medicine*, *48*(6), 749–762. https://doi.org/10.1016/j.freeradbiomed.2009.12.022

Cooper GM. (2000). *The Cell: A Molecular Approach* (2nd ed.). Sunderland (MA): Sinauer Associates. https://www.ncbi.nlm.nih.gov/books/NBK9932/

David, D. C., Hauptmann, S., Scherping, I., Schuessel, K., Keil, U., Rizzu, P., Ravid, R., Dröse, S., Brandt, U., Müller, W. E., Eckert, A., & Götz, J. (2005). Proteomic and Functional Analyses Reveal a Mitochondrial Dysfunction in P301L Tau Transgenic Mice. *Journal of Biological Chemistry*, *280*(25), 23802–23814. https://doi.org/10.1074/jbc.M500356200

Dehmelt, L., & Halpain, S. (2004). The MAP2/Tau family of microtubule-associated proteins. *Genome Biology*, *6*(1), 204. https://doi.org/10.1186/gb-2004-6-1-204

Di Lorenzo, D. (2024). Tau Protein and Tauopathies: Exploring Tau Protein–Protein and Microtubule Interactions, Cross-Interactions and Therapeutic Strategies. *ChemMedChem*, *19*(21). https://doi.org/10.1002/cmdc.202400180

Dickey, C. A., Kamal, A., Lundgren, K., Klosak, N., Bailey, R. M., Dunmore, J., Ash, P., Shoraka, S., Zlatkovic, J., Eckman, C. B., Patterson, C., Dickson, D. W., Nahman, N. S., Hutton, M., Burrows, F., & Petrucelli, L. (2007). The high-affinity HSP90-CHIP complex recognizes and selectively degrades phosphorylated tau client proteins. *Journal of Clinical Investigation*, *117*(3), 648–658. https://doi.org/10.1172/JCI29715

Dixit, R., Ross, J. L., Goldman, Y. E., & Holzbaur, E. L. F. (2008). Differential Regulation of Dynein and Kinesin Motor Proteins by Tau. *Science*, *319*(5866), 1086–1089. https://doi.org/10.1126/science.1152993

Duan, A. R., Jonasson, E. M., Alberico, E. O., Li, C., Scripture, J. P., Miller, R. A., Alber, M. S., & Goodson, H. V. (2017). Interactions between Tau and Different Conformations of Tubulin: Implications for Tau Function and Mechanism. *Journal of Molecular Biology*, *429*(9), 1424–1438. https://doi.org/10.1016/j.jmb.2017.03.018

Dubey, J., Ratnakaran, N., & Koushika, S. P. (2015). Neurodegeneration and microtubule dynamics: death by a thousand cuts. *Frontiers in Cellular Neuroscience*, *9*. https://doi.org/10.3389/fncel.2015.00343

DuBoff, B., Götz, J., & Feany, M. B. (2012). Tau Promotes Neurodegeneration via DRP1 Mislocalization In Vivo. *Neuron*, *75*(4), 618–632. https://doi.org/10.1016/j.neuron.2012.06.026

Duncan, J. E., & Goldstein, L. S. B. (2006). The Genetics of Axonal Transport and Axonal Transport Disorders. *PLoS Genetics*, *2*(9), e124. https://doi.org/10.1371/journal.pgen.0020124

Duong, A., Evstratova, A., Sivitilli, A., Hernandez, J. J., Gosio, J., Wahedi, A., Sondheimer, N., Wrana, J. L., Beaulieu, J.-M., Attisano, L., & Andreazza, A. C. (2021). Characterization of mitochondrial health from human peripheral blood mononuclear cells to cerebral organoids derived from induced pluripotent stem cells. *Scientific Reports*, *11*(1), 4523. https://doi.org/10.1038/s41598-021-84071-6

Ebneth, A., Godemann, R., Stamer, K., Illenberger, S., Trinczek, B., Mandelkow, E.-M., & Mandelkow, E. (1998). Overexpression of Tau Protein Inhibits Kinesin-dependent Trafficking of Vesicles, Mitochondria, and Endoplasmic Reticulum: Implications for Alzheimer's Disease. *The Journal of Cell Biology*, *143*(3), 777–794. https://doi.org/10.1083/jcb.143.3.777

Eckert, A., Nisbet, R., Grimm, A., & Götz, J. (2014). March separate, strike together — Role of phosphorylated TAU in mitochondrial dysfunction in Alzheimer's disease. *Biochimica et Biophysica Acta (BBA) - Molecular Basis of Disease*, *1842*(8), 1258–1266. https://doi.org/10.1016/j.bbadis.2013.08.013

Esteras, N., Kopach, O., Maiolino, M., Lariccia, V., Amoroso, S., Qamar, S., Wray, S., Rusakov, D. A., Jaganjac, M., & Abramov, A. Y. (2022). Mitochondrial ROS control neuronal excitability and cell fate in frontotemporal dementia. *Alzheimer's & Dementia*, *18*(2), 318–338. https://doi.org/10.1002/alz.12394

Esteras, N., Rohrer, J. D., Hardy, J., Wray, S., & Abramov, A. Y. (2017). Mitochondrial hyperpolarization in iPSC-derived neurons from patients of FTDP-17 with 10+16 MAPT mutation leads to oxidative stress and neurodegeneration. *Redox Biology*, *12*, 410–422. https://doi.org/10.1016/j.redox.2017.03.008

Fanara, P., Husted, K. H., Selle, K., Wong, P.-Y. A., Banerjee, J., Brandt, R., & Hellerstein, M. K. (2010). Changes in microtubule turnover accompany synaptic plasticity and memory formation in response to contextual fear conditioning in mice. *Neuroscience*, *168*(1), 167–178. https://doi.org/10.1016/j.neuroscience.2010.03.031

Faw, B. (2003). Pre-frontal executive committee for perception, working memory, attention, long-term memory, motor control, and thinking: A tutorial review. *Consciousness and Cognition*, *12*(1), 83–139. https://doi.org/10.1016/S1053-8100(02)00030-2

Friedhoff, P., von Bergen, M., Mandelkow, E.-M., Davies, P., & Mandelkow, E. (1998). A nucleated assembly mechanism of Alzheimer paired helical filaments. *Proceedings of the National Academy of Sciences*, *95*(26), 15712–15717. https://doi.org/10.1073/pnas.95.26.15712

Goedert, M. (1993). Tau protein and the neurofibrillary pathology of Alzheimer's disease. *Trends in Neurosciences*, *16*(11), 460–465. https://doi.org/10.1016/0166-2236(93)90078-Z

Goedert, M., Crowther, R. A., & Spillantini, M. G. (1998). Tau Mutations Cause Frontotemporal Dementias. *Neuron*, *21*(5), 955–958. https://doi.org/10.1016/S0896-6273(00)80615-7

Goedert, M., Hasegawa, M., Jakes, R., Lawler, S., Cuenda, A., & Cohen, P. (1997). Phosphorylation of microtubule-associated protein tau by stress-activated protein kinases. *FEBS Letters*, *409*(1), 57–62. https://doi.org/10.1016/S0014-5793(97)00483-3

Goedert, M., & Jakes, R. (1990). Expression of separate isoforms of human tau protein: correlation with the tau pattern in brain and effects on tubulin polymerization. *The EMBO Journal*, *9*(13), 4225–4230. https://doi.org/10.1002/j.1460-2075.1990.tb07870.x

Goedert, M., Spillantini, M. G., Cairns, N. J., & Crowther, R. A. (1992). Tau proteins of alzheimer paired helical filaments: Abnormal phosphorylation of all six brain isoforms. *Neuron*, *8*(1), 159–168. https://doi.org/10.1016/0896-6273(92)90117-V

Goedert, M., Spillantini, M. G., Jakes, R., Rutherford, D., & Crowther, R. A. (1989). Multiple isoforms of human microtubule-associated protein tau: sequences and localization in neurofibrillary tangles of Alzheimer's disease. *Neuron*, *3*(4), 519–526. https://doi.org/10.1016/0896-6273(89)90210-9

Gómez-Ramos, A., Díaz-Nido, J., Smith, M. A., Perry, G., & Avila, J. (2003). Effect of the lipid peroxidation product acrolein on tau phosphorylation in neural cells. *Journal of Neuroscience Research*, *71*(6), 863–870. https://doi.org/10.1002/jnr.10525

Gorno-Tempini, M. L., Hillis, A. E., Weintraub, S., Kertesz, A., Mendez, M., Cappa, S. F., Ogar, J. M., Rohrer, J. D., Black, S., Boeve, B. F., Manes, F., Dronkers, N. F., Vandenberghe, R., Rascovsky, K., Patterson, K., Miller, B. L., Knopman, D. S., Hodges, J. R., Mesulam, M. M., & Grossman, M. (2011). Classification of primary progressive aphasia and its variants. *Neurology*, *76*(11), 1006–1014. https://doi.org/10.1212/WNL.0b013e31821103e6

Guha, S., Johnson, G. V. W., & Nehrke, K. (2020). The Crosstalk Between Pathological Tau Phosphorylation and Mitochondrial Dysfunction as a Key to Understanding and Treating Alzheimer's Disease. *Molecular Neurobiology*, *57*(12), 5103–5120. https://doi.org/10.1007/s12035-020-02084-0

Guo, T., Noble, W., & Hanger, D. P. (2017). Roles of tau protein in health and disease. *Acta Neuropathologica*, *133*(5), 665–704. https://doi.org/10.1007/s00401-017-1707-9

Guo, X., Macleod, G. T., Wellington, A., Hu, F., Panchumarthi, S., Schoenfield, M., Marin, L., Charlton, M. P., Atwood, H. L., & Zinsmaier, K. E. (2005). The GTPase dMiro Is Required for Axonal Transport of Mitochondria to Drosophila Synapses. *Neuron*, *47*(3), 379–393. https://doi.org/10.1016/j.neuron.2005.06.027

Hanger, D. P., Anderton, B. H., & Noble, W. (2009). Tau phosphorylation: the therapeutic challenge for neurodegenerative disease. *Trends in Molecular Medicine*, *15*(3), 112–119. https://doi.org/10.1016/j.molmed.2009.01.003

Harada, A., Oguchi, K., Okabe, S., Kuno, J., Terada, S., Ohshima, T., Sato-Yoshitake, R., Takei, Y., Noda, T., & Hirokawa, N. (1994). Altered microtubule organization in small-calibre axons of mice lacking tau protein. *Nature*, *369*(6480), 488–491. https://doi.org/10.1038/369488a0

Hasegawa, M., Smith, M. J., Iijima, M., Tabira, T., & Goedert, M. (1999). FTDP-17 mutations N279K and S305N in tau produce increased splicing of exon 10. *FEBS Letters*, *443*(2), 93–96. https://doi.org/10.1016/S0014-5793(98)01696-2

Hayashi, J., Ohta, S., Kikuchi, A., Takemitsu, M., Goto, Y., & Nonaka, I. (1991). Introduction of disease-related mitochondrial DNA deletions into HeLa cells lacking mitochondrial DNA results in mitochondrial dysfunction. *Proceedings of the National Academy of Sciences*, *88*(23), 10614–10618. https://doi.org/10.1073/pnas.88.23.10614

Hendriks, S., Peetoom, K., Bakker, C., van der Flier, W. M., Papma, J. M., Koopmans, R., Verhey, F. R. J., de Vugt, M., Köhler, S., Withall, A., Parlevliet, J. L., Uysal-Bozkir, Ö., Gibson, R. C., Neita, S. M., Nielsen, T. R., Salem, L. C., Nyberg, J., Lopes, M. A., Dominguez, J. C., … Ruano, L. (2021). Global Prevalence of Young-Onset Dementia. *JAMA Neurology*, *78*(9), 1080. https://doi.org/10.1001/jamaneurol.2021.2161

Himmler, A. (1989). Structure of the Bovine Tau Gene: Alternatively Spliced Transcripts Generate a Protein Family. *Molecular and Cellular Biology*, *9*(4), 1389–1396. https://doi.org/10.1128/mcb.9.4.1389-1396.1989

Hodges, J. R., & Patterson, K. (2007). Semantic dementia: a unique clinicopathological syndrome. *The Lancet Neurology*, *6*(11), 1004–1014. https://doi.org/10.1016/S1474-4422(07)70266-1

Hofhaus, G., Weiss, H., & Leonard, K. (1991). Electron microscopic analysis of the peripheral and membrane parts of mitochondrial NADH dehydrogenase (Complex I). *Journal of Molecular Biology*, *221*(3), 1027–1043. https://doi.org/10.1016/0022-2836(91)80190-6

Hong, M. (1998). Mutation-Specific Functional Impairments in Distinct Tau Isoforms of Hereditary FTDP-17. *Science*, *282*(5395), 1914–1917. https://doi.org/10.1126/science.282.5395.1914

Hoover, B. R., Reed, M. N., Su, J., Penrod, R. D., Kotilinek, L. A., Grant, M. K., Pitstick, R., Carlson, G. A., Lanier, L. M., Yuan, L.-L., Ashe, K. H., & Liao, D. (2010). Tau Mislocalization to Dendritic Spines Mediates Synaptic Dysfunction Independently of Neurodegeneration. *Neuron*, *68*(6), 1067–1081. https://doi.org/10.1016/j.neuron.2010.11.030

Horio, T., & Murata, T. (2014). The role of dynamic instability in microtubule organization. *Frontiers in Plant Science*, *5*. https://doi.org/10.3389/fpls.2014.00511

Hu, Y., Li, X.-C., Wang, Z., Luo, Y., Zhang, X., Liu, X.-P., Feng, Q., Wang, Q., Yue, Z., Chen, Z., Ye, K., Wang, J.-Z., & Liu, G.-P. (2016). Tau accumulation impairs mitophagy *via* increasing mitochondrial membrane potential and reducing mitochondrial Parkin. *Oncotarget*, *7*(14), 17356–17368. https://doi.org/10.18632/oncotarget.7861

Hutton, M., Lendon, C. L., Rizzu, P., Baker, M., Froelich, S., Houlden, H., Pickering-Brown, S., Chakraverty, S., Isaacs, A., Grover, A., Hackett, J., Adamson, J., Lincoln, S., Dickson, D., Davies, P., Petersen, R. C., Stevens, M., de Graaff, E., Wauters, E., … Heutink, P. (1998). Association of missense and 5′-splice-site mutations in tau with the inherited dementia FTDP-17. *Nature*, *393*(6686), 702–705. https://doi.org/10.1038/31508

Ibáñez-Salazar, A., Bañuelos-Hernández, B., Rodríguez-Leyva, I., Chi-Ahumada, E., Monreal-Escalante, E., Jiménez-Capdeville, M. E., & Rosales-Mendoza, S. (2017). Oxidative Stress Modifies the Levels and Phosphorylation State of Tau Protein in Human Fibroblasts. *Frontiers in Neuroscience*, *11*. https://doi.org/10.3389/fnins.2017.00495

Iqbal, K., del C. Alonso, A., Chen, S., Chohan, M. O., El-Akkad, E., Gong, C.-X., Khatoon, S., Li, B., Liu, F., Rahman, A., Tanimukai, H., & Grundke-Iqbal, I. (2005). Tau pathology in Alzheimer disease and other tauopathies. *Biochimica et Biophysica Acta (BBA) - Molecular Basis of Disease*, *1739*(2–3), 198–210. https://doi.org/10.1016/j.bbadis.2004.09.008

Ittner, L. M., Fath, T., Ke, Y. D., Bi, M., van Eersel, J., Li, K. M., Gunning, P., & Götz, J. (2008). Parkinsonism and impaired axonal transport in a mouse model of frontotemporal dementia. *Proceedings of the National Academy of Sciences*, *105*(41), 15997–16002. https://doi.org/10.1073/pnas.0808084105

Janke, C., & Magiera, M. M. (2020). The tubulin code and its role in controlling microtubule properties and functions. *Nature Reviews Molecular Cell Biology*, *21*(6), 307–326. https://doi.org/10.1038/s41580-020-0214-3

Josephs, K. A., Hodges, J. R., Snowden, J. S., Mackenzie, I. R., Neumann, M., Mann, D. M., & Dickson, D. W. (2011). Neuropathological background of phenotypical variability in frontotemporal dementia. *Acta Neuropathologica*, *122*(2), 137–153. https://doi.org/10.1007/s00401-011-0839-6

Jucker, M., & Walker, L. C. (2013). Self-propagation of pathogenic protein aggregates in neurodegenerative diseases. *Nature*, *501*(7465), 45–51. https://doi.org/10.1038/nature12481

Kanwisher, N., McDermott, J., & Chun, M. M. (1997). The Fusiform Face Area: A Module in Human Extrastriate Cortex Specialized for Face Perception. *The Journal of Neuroscience*, *17*(11), 4302–4311. https://doi.org/10.1523/JNEUROSCI.17-11-04302.1997

Katrukha, E. A., Jurriens, D., Salas Pastene, D. M., & Kapitein, L. C. (2021). Quantitative mapping of dense microtubule arrays in mammalian neurons. *ELife*, *10*. https://doi.org/10.7554/eLife.67925

Kiernan, J. A. (2012). Anatomy of the Temporal Lobe. *Epilepsy Research and Treatment*, *2012*, 1–12. https://doi.org/10.1155/2012/176157

Knott, A. B., Perkins, G., Schwarzenbacher, R., & Bossy-Wetzel, E. (2008). Mitochondrial fragmentation in neurodegeneration. *Nature Reviews Neuroscience*, *9*(7), 505–518. https://doi.org/10.1038/nrn2417

Kopeikina, K. J., Carlson, G. A., Pitstick, R., Ludvigson, A. E., Peters, A., Luebke, J. I., Koffie, R. M., Frosch, M. P., Hyman, B. T., & Spires-Jones, T. L. (2011). Tau Accumulation Causes

Mitochondrial Distribution Deficits in Neurons in a Mouse Model of Tauopathy and in Human Alzheimer's Disease Brain. *The American Journal of Pathology*, *179*(4), 2071–2082. https://doi.org/10.1016/j.ajpath.2011.07.004

Kovacs, G. G., Pittman, A., Revesz, T., Luk, C., Lees, A., Kiss, E., Tariska, P., Laszlo, L., Molnár, K., Molnar, M. J., Tolnay, M., & de Silva, R. (2008). MAPT S305I mutation: implications for argyrophilic grain disease. *Acta Neuropathologica*, *116*(1), 103–118. https://doi.org/10.1007/s00401-007-0322-6

Kravitz, D. J., Saleem, K. S., Baker, C. I., Ungerleider, L. G., & Mishkin, M. (2013). The ventral visual pathway: an expanded neural framework for the processing of object quality. *Trends in Cognitive Sciences*, *17*(1), 26–49. https://doi.org/10.1016/j.tics.2012.10.011

Kurz, A., Kurz, C., Ellis, K., & Lautenschlager, N. T. (2014). What is frontotemporal dementia? *Maturitas*, *79*(2), 216–219. https://doi.org/10.1016/j.maturitas.2014.07.001

Kussmaul, L., & Hirst, J. (2006). The mechanism of superoxide production by NADH:ubiquinone oxidoreductase (complex I) from bovine heart mitochondria. *Proceedings of the National Academy of Sciences*, *103*(20), 7607–7612. https://doi.org/10.1073/pnas.0510977103

Ludikhuize, M. C., Meerlo, M., Burgering, B. M. T., & Rodríguez Colman, M. J. (2021). Protocol to profile the bioenergetics of organoids using Seahorse. *STAR Protocols*, *2*(1), 100386. https://doi.org/10.1016/j.xpro.2021.100386

Mackenzie, I. R. A., Munoz, D. G., Kusaka, H., Yokota, O., Ishihara, K., Roeber, S., Kretzschmar, H. A., Cairns, N. J., & Neumann, M. (2011). Distinct pathological subtypes of FTLD-FUS. *Acta Neuropathologica*, *121*(2), 207–218. https://doi.org/10.1007/s00401-010-0764-0

Mackenzie, I. R. A., & Neumann, M. (2016). Molecular neuropathology of frontotemporal dementia: insights into disease mechanisms from postmortem studies. *Journal of Neurochemistry*, *138*(S1), 54–70. https://doi.org/10.1111/jnc.13588

Magiera, M. M., & Janke, C. (2014). Post-translational modifications of tubulin. *Current Biology*, *24*(9), R351–R354. https://doi.org/10.1016/j.cub.2014.03.032

Manczak, M., & Reddy, P. H. (2012). Abnormal interaction between the mitochondrial fission protein Drp1 and hyperphosphorylated tau in Alzheimer's disease neurons: implications for mitochondrial dysfunction and neuronal damage. *Human Molecular Genetics*, *21*(11), 2538–2547. https://doi.org/10.1093/hmg/dds072

Martin, L., Latypova, X., & Terro, F. (2011). Post-translational modifications of tau protein: Implications for Alzheimer's disease. *Neurochemistry International*, *58*(4), 458–471. https://doi.org/10.1016/j.neuint.2010.12.023

Meraz-Ríos, M. A., Lira-De León, K. I., Campos-Peña, V., De Anda-Hernández, M. A., & Mena-López, R. (2010). Tau oligomers and aggregation in Alzheimer's disease. *Journal of Neurochemistry*, *112*(6), 1353–1367. https://doi.org/10.1111/j.1471-4159.2009.06511.x

Mietelska-Porowska, A., Wasik, U., Goras, M., Filipek, A., & Niewiadomska, G. (2014). Tau Protein Modifications and Interactions: Their Role in Function and Dysfunction. *International Journal of Molecular Sciences*, *15*(3), 4671–4713. https://doi.org/10.3390/ijms15034671

Mitchison, T., & Kirschner, M. (1984). Dynamic instability of microtubule growth. *Nature*, *312*(5991), 237–242. https://doi.org/10.1038/312237a0

Mok, S.-A., Condello, C., Freilich, R., Gillies, A., Arhar, T., Oroz, J., Kadavath, H., Julien, O., Assimon, V. A., Rauch, J. N., Dunyak, B. M., Lee, J., Tsai, F. T. F., Wilson, M. R., Zweckstetter, M., Dickey, C. A., & Gestwicki, J. E. (2018). Mapping interactions with the chaperone network reveals factors that protect against tau aggregation. *Nature Structural & Molecular Biology*, *25*(5), 384–393. https://doi.org/10.1038/s41594-018-0057-1

Moreno, H., Morfini, G., Buitrago, L., Ujlaki, G., Choi, S., Yu, E., Moreira, J. E., Avila, J., Brady, S. T., Pant, H., Sugimori, M., & Llinás, R. R. (2016). Tau pathology-mediated presynaptic dysfunction. *Neuroscience*, *325*, 30–38. https://doi.org/10.1016/j.neuroscience.2016.03.044

Neumann, M., Rademakers, R., Roeber, S., Baker, M., Kretzschmar, H. A., & Mackenzie, I. R. A. (2009). A new subtype of frontotemporal lobar degeneration with FUS pathology. *Brain*, *132*(11), 2922–2931. https://doi.org/10.1093/brain/awp214

Neumann, M., Sampathu, D. M., Kwong, L. K., Truax, A. C., Micsenyi, M. C., Chou, T. T., Bruce, J., Schuck, T., Grossman, M., Clark, C. M., McCluskey, L. F., Miller, B. L., Masliah, E., Mackenzie, I. R., Feldman, H., Feiden, W., Kretzschmar, H. A., Trojanowski, J. Q., & Lee, V. M.-Y. (2006). Ubiquitinated TDP-43 in Frontotemporal Lobar Degeneration and Amyotrophic Lateral Sclerosis. *Science*, *314*(5796), 130–133. https://doi.org/10.1126/science.1134108

Noble, W., Hanger, D. P., Miller, C. C. J., & Lovestone, S. (2013). The Importance of Tau Phosphorylation for Neurodegenerative Diseases. *Frontiers in Neurology*, *4*. https://doi.org/10.3389/fneur.2013.00083

Pérez, M., Cuadros, R., Smith, M. A., Perry, G., & Avila, J. (2000). Phosphorylated, but not native, tau protein assembles following reaction with the lipid peroxidation product, 4-hydroxy-2-nonenal. *FEBS Letters*, *486*(3), 270–274. https://doi.org/10.1016/S0014-5793(00)02323-1

Peris, L., Parato, J., Qu, X., Soleilhac, J. M., Lanté, F., Kumar, A., Pero, M. E., Martínez-Hernández, J., Corrao, C., Falivelli, G., Payet, F., Gory-Fauré, S., Bosc, C., Blanca Ramirez, M., Sproul, A., Brocard, J., Di Cara, B., Delagrange, P., Buisson, A., … Andrieux, A. (2022).

Tubulin tyrosination regulates synaptic function and is disrupted in Alzheimer's disease. *Brain*, *145*(7), 2486–2506. https://doi.org/10.1093/brain/awab436

Perry, R. J., Graham, A., Williams, G., Rosen, H., Erzinçlioglu, S., Weiner, M., Miller, B., & Hodges, J. (2006). Patterns of Frontal Lobe Atrophy in Frontotemporal Dementia: A Volumetric MRI Study. *Dementia and Geriatric Cognitive Disorders*, *22*(4), 278–287. https://doi.org/10.1159/000095128

Petrucelli, L. (2004). CHIP and Hsp70 regulate tau ubiquitination, degradation and aggregation. *Human Molecular Genetics*, *13*(7), 703–714. https://doi.org/10.1093/hmg/ddh083

Picard, M. (2015). Mitochondrial synapses: intracellular communication and signal integration. *Trends in Neurosciences*, *38*(8), 468–474. https://doi.org/10.1016/j.tins.2015.06.001

Portran, D., Schaedel, L., Xu, Z., Théry, M., & Nachury, M. V. (2017). Tubulin acetylation protects long-lived microtubules against mechanical ageing. *Nature Cell Biology*, *19*(4), 391–398. https://doi.org/10.1038/ncb3481

Qiang, L., Sun, X., Austin, T. O., Muralidharan, H., Jean, D. C., Liu, M., Yu, W., & Baas, P. W. (2018). Tau Does Not Stabilize Axonal Microtubules but Rather Enables Them to Have Long Labile Domains. *Current Biology : CB*, *28*(13), 2181-2189.e4. https://doi.org/10.1016/j.cub.2018.05.045

Rohrer, J. D., Ridgway, G. R., Crutch, S. J., Hailstone, J., Goll, J. C., Clarkson, M. J., Mead, S., Beck, J., Mummery, C., Ourselin, S., Warrington, E. K., Rossor, M. N., & Warren, J. D. (2010). Progressive logopenic/phonological aphasia: Erosion of the language network. *NeuroImage*, *49*(1), 984–993. https://doi.org/10.1016/j.neuroimage.2009.08.002

Rohrer, J. D., Rossor, M. N., & Warren, J. D. (2010). Syndromes of nonfluent primary progressive aphasia. *Neurology*, *75*(7), 603–610. https://doi.org/10.1212/WNL.0b013e3181ed9c6b

Rohrer, J. D., Warren, J. D., Modat, M., Ridgway, G. R., Douiri, A., Rossor, M. N., Ourselin, S., & Fox, N. C. (2009). Patterns of cortical thinning in the language variants of frontotemporal lobar degeneration. *Neurology*, *72*(18), 1562–1569. https://doi.org/10.1212/WNL.0b013e3181a4124e

Rösler, T. W., Tayaranian Marvian, A., Brendel, M., Nykänen, N.-P., Höllerhage, M., Schwarz, S. C., Hopfner, F., Koeglsperger, T., Respondek, G., Schweyer, K., Levin, J., Villemagne, V. L., Barthel, H., Sabri, O., Müller, U., Meissner, W. G., Kovacs, G. G., & Höglinger, G. U. (2019). Four-repeat tauopathies. *Progress in Neurobiology*, *180*, 101644. https://doi.org/10.1016/j.pneurobio.2019.101644

Saitoh, M., Nishitoh, H., Fujii, M., Takeda, K., Tobiume, K., Sawada, Y., Kawabata, M., Miyazono, K., & Ichijo, H. (1998). Mammalian thioredoxin is a direct inhibitor of apoptosis

signal-regulating kinase (ASK) 1. *The EMBO Journal*, *17*(9), 2596–2606. https://doi.org/10.1093/emboj/17.9.2596

Santarella, R. A., Skiniotis, G., Goldie, K. N., Tittmann, P., Gross, H., Mandelkow, E.-M., Mandelkow, E., & Hoenger, A. (2004). Surface-decoration of Microtubules by Human Tau. *Journal of Molecular Biology*, *339*(3), 539–553. https://doi.org/10.1016/j.jmb.2004.04.008

Sato, C., Barthélemy, N. R., Mawuenyega, K. G., Patterson, B. W., Gordon, B. A., Jockel-Balsarotti, J., Sullivan, M., Crisp, M. J., Kasten, T., Kirmess, K. M., Kanaan, N. M., Yarasheski, K. E., Baker-Nigh, A., Benzinger, T. L. S., Miller, T. M., Karch, C. M., & Bateman, R. J. (2018). Tau Kinetics in Neurons and the Human Central Nervous System. *Neuron*, *97*(6), 1284-1298.e7. https://doi.org/10.1016/j.neuron.2018.02.015

Schulz, K. L., Eckert, A., Rhein, V., Mai, S., Haase, W., Reichert, A. S., Jendrach, M., Müller, W. E., & Leuner, K. (2012). A New Link to Mitochondrial Impairment in Tauopathies. *Molecular Neurobiology*, *46*(1), 205–216. https://doi.org/10.1007/s12035-012-8308-3

Schwarz, T. L. (2013). Mitochondrial Trafficking in Neurons. *Cold Spring Harbor Perspectives in Biology*, *5*(6), a011304–a011304. https://doi.org/10.1101/cshperspect.a011304

Shahpasand, K., Uemura, I., Saito, T., Asano, T., Hata, K., Shibata, K., Toyoshima, Y., Hasegawa, M., & Hisanaga, S. (2012). Regulation of Mitochondrial Transport and Inter-Microtubule Spacing by Tau Phosphorylation at the Sites Hyperphosphorylated in Alzheimer's Disease. *The Journal of Neuroscience*, *32*(7), 2430–2441. https://doi.org/10.1523/JNEUROSCI.5927-11.2012

Sloan, S. A., Darmanis, S., Huber, N., Khan, T. A., Birey, F., Caneda, C., Reimer, R., Quake, S. R., Barres, B. A., & Paşca, S. P. (2017). Human Astrocyte Maturation Captured in 3D Cerebral Cortical Spheroids Derived from Pluripotent Stem Cells. *Neuron*, *95*(4), 779-790.e6. https://doi.org/10.1016/j.neuron.2017.07.035

Soppina, V., Herbstman, J. F., Skiniotis, G., & Verhey, K. J. (2012). Luminal Localization of α-tubulin K40 Acetylation by Cryo-EM Analysis of Fab-Labeled Microtubules. *PLoS ONE*, *7*(10), e48204. https://doi.org/10.1371/journal.pone.0048204

Sposito, T., Preza, E., Mahoney, C. J., Setó-Salvia, N., Ryan, N. S., Morris, H. R., Arber, C., Devine, M. J., Houlden, H., Warner, T. T., Bushell, T. J., Zagnoni, M., Kunath, T., Livesey, F. J., Fox, N. C., Rossor, M. N., Hardy, J., & Wray, S. (2015). Developmental regulation of tau splicing is disrupted in stem cell-derived neurons from frontotemporal dementia patients with the 10 + 16 splice-site mutation in MAPT. *Human Molecular Genetics*, *24*(18), 5260–5269. https://doi.org/10.1093/hmg/ddv246

Srivastava, A. P., Luo, M., Zhou, W., Symersky, J., Bai, D., Chambers, M. G., Faraldo-Gómez, J. D., Liao, M., & Mueller, D. M. (2018). High-resolution cryo-EM analysis of the yeast ATP synthase in a lipid membrane. *Science*, *360*(6389). https://doi.org/10.1126/science.aas9699

Stamer, K., Vogel, R., Thies, E., Mandelkow, E., & Mandelkow, E.-M. (2002). Tau blocks traffic of organelles, neurofilaments, and APP vesicles in neurons and enhances oxidative stress. *The Journal of Cell Biology*, *156*(6), 1051–1063. https://doi.org/10.1083/jcb.200108057

Stanford, P. M., Halliday, G. M., Brooks, W. S., Kwok, J. B. J., Storey, C. E., Creasey, H., Morris, J. G. L., Fulham, M. J., & Schofield, P. R. (2000). Progressive supranuclear palsy pathology caused by a novel silent mutation in exon 10 of the tau gene. *Brain*, *123*(5), 880–893. https://doi.org/10.1093/brain/123.5.880

Stowers, R. S., Megeath, L. J., Górska-Andrzejak, J., Meinertzhagen, I. A., & Schwarz, T. L. (2002). Axonal Transport of Mitochondria to Synapses Depends on Milton, a Novel Drosophila Protein. *Neuron*, *36*(6), 1063–1077. https://doi.org/10.1016/S0896-6273(02)01094-2

Sullivan, K. F. (1988). Structure and Utilization of Tubulin Isotypes. *Annual Review of Cell Biology*, *4*(1), 687–716. https://doi.org/10.1146/annurev.cb.04.110188.003351

Sun, F., Huo, X., Zhai, Y., Wang, A., Xu, J., Su, D., Bartlam, M., & Rao, Z. (2005). Crystal Structure of Mitochondrial Respiratory Membrane Protein Complex II. *Cell*, *121*(7), 1043–1057. https://doi.org/10.1016/j.cell.2005.05.025

Szabo, L., Eckert, A., & Grimm, A. (2020a). Insights into Disease-Associated Tau Impact on Mitochondria. *International Journal of Molecular Sciences*, *21*(17), 6344. https://doi.org/10.3390/ijms21176344

Szabo, L., Eckert, A., & Grimm, A. (2020b). Insights into Disease-Associated Tau Impact on Mitochondria. *International Journal of Molecular Sciences*, *21*(17), 6344. https://doi.org/10.3390/ijms21176344

Tas, R. P., Chazeau, A., Cloin, B. M. C., Lambers, M. L. A., Hoogenraad, C. C., & Kapitein, L. C. (2017). Differentiation between Oppositely Oriented Microtubules Controls Polarized Neuronal Transport. *Neuron*, *96*(6), 1264-1271.e5. https://doi.org/10.1016/j.neuron.2017.11.018

Terwel, D., Dewachter, I., & Van Leuven, F. (2002). Axonal Transport, Tau Protein, and Neurodegeneration in Alzheimer's Disease. *NeuroMolecular Medicine*, *2*(2), 151–166. https://doi.org/10.1385/NMM:2:2:151

Torres, A. K., Jara, C., Olesen, M. A., & Tapia-Rojas, C. (2021). Pathologically phosphorylated tau at S396/404 (PHF-1) is accumulated inside of hippocampal synaptic mitochondria of aged Wild-type mice. *Scientific Reports*, *11*(1), 4448. https://doi.org/10.1038/s41598-021-83910-w

Trabzuni, D., Wray, S., Vandrovcova, J., Ramasamy, A., Walker, R., Smith, C., Luk, C., Gibbs, J. R., Dillman, A., Hernandez, D. G., Arepalli, S., Singleton, A. B., Cookson, M. R., Pittman, A. M., de Silva, R., Weale, M. E., Hardy, J., & Ryten, M. (2012). MAPT expression and splicing is differentially regulated by brain region: relation to genotype and implication for tauopathies. *Human Molecular Genetics*, *21*(18), 4094–4103. https://doi.org/10.1093/hmg/dds238

Tracy, T. E., Madero-Pérez, J., Swaney, D. L., Chang, T. S., Moritz, M., Konrad, C., Ward, M. E., Stevenson, E., Hüttenhain, R., Kauwe, G., Mercedes, M., Sweetland-Martin, L., Chen, X., Mok, S.-A., Wong, M. Y., Telpoukhovskaia, M., Min, S.-W., Wang, C., Sohn, P. D., … Gan, L. (2022). Tau interactome maps synaptic and mitochondrial processes associated with neurodegeneration. *Cell*, *185*(4), 712-728.e14. https://doi.org/10.1016/j.cell.2021.12.041

Urrestizala-Arenaza, N., Cerchio, S., Cavaliere, F., & Magliaro, C. (2024). Limitations of human brain organoids to study neurodegenerative diseases: a manual to survive. *Frontiers in Cellular Neuroscience*, *18*. https://doi.org/10.3389/fncel.2024.1419526

Urso, D., Giannoni-Luza, S., Brayne, C., Ray, N., & Logroscino, G. (2025). Incidence and Prevalence of Frontotemporal Dementia. *JAMA Neurology*, *82*(11), 1144. https://doi.org/10.1001/jamaneurol.2025.3307

Varani, L., Hasegawa, M., Spillantini, M. G., Smith, M. J., Murrell, J. R., Ghetti, B., Klug, A., Goedert, M., & Varani, G. (1999). Structure of tau exon 10 splicing regulatory element RNA and destabilization by mutations of frontotemporal dementia and parkinsonism linked to chromosome 17. *Proceedings of the National Academy of Sciences*, *96*(14), 8229–8234. https://doi.org/10.1073/pnas.96.14.8229

Verhey, K. J., & Gaertig, J. (2007). The Tubulin Code. *Cell Cycle*, *6*(17), 2152–2160. https://doi.org/10.4161/cc.6.17.4633

Verheyen, A., Diels, A., Reumers, J., Van Hoorde, K., Van den Wyngaert, I., van Outryve d'Ydewalle, C., De Bondt, A., Kuijlaars, J., De Muynck, L., De Hoogt, R., Bretteville, A., Jaensch, S., Buist, A., Cabrera-Socorro, A., Wray, S., Ebneth, A., Roevens, P., Royaux, I., & Peeters, P. J. (2018). Genetically Engineered iPSC-Derived FTDP-17 MAPT Neurons Display Mutation-Specific Neurodegenerative and Neurodevelopmental Phenotypes. *Stem Cell Reports*, *11*(2), 363–379. https://doi.org/10.1016/j.stemcr.2018.06.022

von Bergen, M., Friedhoff, P., Biernat, J., Heberle, J., Mandelkow, E. M., & Mandelkow, E. (2000). Assembly of tau protein into Alzheimer paired helical filaments depends on a local sequence

motif ((306)VQIVYK(311)) forming beta structure. *Proceedings of the National Academy of Sciences of the United States of America*, *97*(10), 5129–5134. https://doi.org/10.1073/pnas.97.10.5129

Warren, J. D., Rohrer, J. D., & Rossor, M. N. (2013). Frontotemporal dementia. *BMJ*, *347*(aug12 3), f4827–f4827. https://doi.org/10.1136/bmj.f4827

Whitwell, J. L., Jack, C. R., Boeve, B. F., Senjem, M. L., Baker, M., Ivnik, R. J., Knopman, D. S., Wszolek, Z. K., Petersen, R. C., Rademakers, R., & Josephs, K. A. (2009). Atrophy patterns in IVS10+16, IVS10+3, N279K, S305N, P301L, and V337M *MAPT* mutations. *Neurology*, *73*(13), 1058–1065. https://doi.org/10.1212/WNL.0b013e3181b9c8b9

Wikström, M. (1984). Two protons are pumped from the mitochondrial matrix per electron transferred between NADH and ubiquinone. *FEBS Letters*, *169*(2), 300–304. https://doi.org/10.1016/0014-5793(84)80338-5

Wirth, C., Brandt, U., Hunte, C., & Zickermann, V. (2016). Structure and function of mitochondrial complex I. *Biochimica et Biophysica Acta (BBA) - Bioenergetics*, *1857*(7), 902–914. https://doi.org/10.1016/j.bbabio.2016.02.013

Xia, D., Yu, C.-A., Kim, H., Xia, J.-Z., Kachurin, A. M., Zhang, L., Yu, L., & Deisenhofer, J. (1997). Crystal Structure of the Cytochrome bc $_1$ Complex from Bovine Heart Mitochondria. *Science*, *277*(5322), 60–66. https://doi.org/10.1126/science.277.5322.60

Xu, Y., Xue, D., Bankhead, A., & Neamati, N. (2020). Why All the Fuss about Oxidative Phosphorylation (OXPHOS)? *Journal of Medicinal Chemistry*, *63*(23), 14276–14307. https://doi.org/10.1021/acs.jmedchem.0c01013

Yang, J., Zhi, W., & Wang, L. (2024). Role of Tau Protein in Neurodegenerative Diseases and Development of Its Targeted Drugs: A Literature Review. *Molecules*, *29*(12), 2812. https://doi.org/10.3390/molecules29122812

Yoo, I., Ahn, I., Lee, J., & Lee, N. (2024). Extracellular flux assay (Seahorse assay): Diverse applications in metabolic research across biological disciplines. *Molecules and Cells*, *47*(8), 100095. https://doi.org/10.1016/j.mocell.2024.100095

Zhu, X., Rottkamp, C. A., Boux, H., Takeda, A., Perry, G., & Smith, M. A. (2000). Activation of p38 Kinase Links Tau Phosphorylation, Oxidative Stress, and Cell Cycle-Related Events in Alzheimer Disease. *Journal of Neuropathology & Experimental Neurology*, *59*(10), 880–888. https://doi.org/10.1093/jnen/59.10.880

8. Acknowledgements

Completing my master's thesis would not have been possible without the support surrounding me. First, I would like to thank dr. Kathryn Bowles for the opportunity to perform my internship at her lab. I greatly appreciate her guidance, feedback and mentorship throughout my internship and after. Next, I want to give a huge thank you to every member of the Bowles lab and everyone I worked with at the UK-DRI in Edinburgh. A special thanks to my internal supervisor, Professor Morella. Lastly, I want to thank my family and friends for the support.